Masonry columns confined with fabric reinforced cementitious matrix (FRCM) systems: A round robin test

Published Version:
Masonry columns confined with fabric reinforced cementitious matrix (FRCM) systems: A round robin test / Aiello M.A.; Bencardino F.; Cascardi A.; D'Antino T.; Fagone M.; Frana I.; La Mendola L.; Lignola G.P.; Mazzotti C.; Micelli F.; Minafo G.; Napoli A.; Ombres L.; Oddo M.C.; Poggi C.; Prota A.; Ramaglia G.; Ranocchiai G.; Realfonzo R.; Verre S.. - In: CONSTRUCTION AND BUILDING MATERIALS. - ISSN 0950-0618. - ELETTRONICO. - 298:(2021), pp. 123816.1-123816.31. [10.1016/j.conbuildmat.2021.123816]

This version is available at: https://hdl.handle.net/11585/860381 since: 2022-02-17

Published:

DOI: http://doi.org/10.1016/j.conbuildmat.2021.123816

MASONRY COLUMNS CONFINED WITH FABRIC REINFORCED CEMENTITIOUS MATRIX SYSTEMS: A ROUND ROBIN TEST

Aiello M.A [1], Bencardino F.[2], Cascardi A.[3], D'Antino T.[4], Fagone M.[5], Frana, I.[10], La Mendola L.[7], Lignola G.P.[8], Mazzotti C.[6], Micelli F.[1], Minafò G.[7], Napoli A.[9], Ombres L[2]., Oddo M.C.[7], Poggi C.[4], Protа A.[8], Ramaglia G.[8], Ranocchia G.[5], Realfonzo R.[9], Verre S[2]*

[1]University of Salento, Department of Innovation Engineering, via per Monteroni, Lecce – 73100, Italy;

[2]University of Calabria, Department of Civil Engineering, 87036 Cosenza, Italy;

[3]ITC-CNR, Construction Technologies Institute - Italian National Research Council, Bari – 70124, Italy;

[4]Politecnico di Milano, Department of Architecture, Built Environment and Construction Engineering, P.zza L. da Vinci 32, 20133 Milan, Italy;

[5]University of Florence, Department of Civil and Environmental Engineering, DICEA, Via di S. Marta 3, 50139 Florence, Italy;

[6]University of Bologna, Department of Civil, Chemical, Environmental and Materials Engineering, DICAM, Viale Risorgimento 2, 40136 Bologna, Italy;

[7]University of Palermo, Engineering Department, Viale delle Scienze, 90128 Palermo, Italy;

[8]University of Naples ''Federico II", Department of Structures for Engineering and Architecture, via Claudio 21, 80125 Naples, Italy;

[9]University of Salerno, Department of Civil Engineering, Via Giovanni Paolo II, 132, 84084 Fisciano, SA, Italy;

[10]University of Bologna, CIRI Buildings and Construction, Via del Lazzaretto 15/5, 40131 Bologna, Italy.

*corresponding author

List of symbols

The symbols used within the paper are reported herein:

- A_c is the net cross-sectional area of the compressed member (mm^2);
- A_e is the cross-sectional area effectively confined (mm^2);
- A_f is the cross-sectional area of the dry fabric (mm^2);
- b and h are the short and long side dimensions of the compressed member with rectangular cross section (mm);
- CoV is the coefficient of variation;
- E_1 is the modulus of elasticity of uncracked FRCM (MPa);
- E_2 is the modulus of the cracked FRCM (MPa);
- E_f is the Young's modulus of the dry fabric (MPa);
- $f_{c,m}$ is the average compressive strength of the masonry and its constituents reported in Table 3 (MPa);
- $f_{c,mat}$ is the compressive strength of the FRCM-mortar (MPa);
- f_l is the maximum confinement pressure (MPa);
- $f_{l,eff}$ is the effective confinement pressure (MPa);
- F_{max} is the maximum recorded load during the test (N);
- $f_{c,m,exp}$ is the experimental compressive strength of the masonry column (MPa);

- $f_{c,m,pred}$ is the predicted compressive strength of the masonry column (MPa);
- f_{mcd} is the design compressive strength of confined masonry column (MPa);
- f_{md} is the design compressive strength of unconfined masonry column (MPa);
- g_m is the mass density of the masonry (kg/m^3);
- k' is the dimensionless coefficients for strength increment;
- k_a is the shape factor;
- k_H is the dimensionless coefficient of efficiency in the horizontal direction;
- k_{mat} is the dimensionless coefficient accounting for the effect of inorganic matrix;
- n is the number of fabric layers (-);
- P is the axial load applied during the compressive test of the column (N);
- P_{cr} is the first axial cracking load of the column;
- r_c is the corner radius of the column;
- s is the maximum slip recorded during the lap shear test (mm);
- t_f is the equivalent thickness of the fabric (mm);
- t_{mat} is the total thickness of the FRCM (mm);
- α_1, α_2 and α_3 are the strength increment coefficients (-);
- γ_m is the partial factor for materials and products;
- ε_{fd} is the design tensile strain of the FRCM (-);
- ε_{fe} is the effective ultimate tensile strain of the FRCM (-);
- ε_H is the lateral strain of the columns (-);
- $\varepsilon_{lim,conv}$ is the conventional strain limit defined by bond test (-);
- ε_u is the ultimate tensile strain of the FRCM (-):
- $\varepsilon_{u,f}$ is the ultimate tensile strain of the fabric (-);
- ε_V is the vertical strain of the columns (-);
- η_a is the environmental conversion factor (-);
- ρ_{mat} is the matrix reinforcement ratio (-);
- $\sigma_{lim,b}$ is the conventional stress limit of the FRCM (MPa):
- $\sigma_{lim,conv}$ is the mean conventional stress limit (MPa);
- σ_t is the tensile stress in the FRCM in Fig. 7 (MPa);
- σ_u is the ultimate tensile stress of the FRCM (MPa);
- $\sigma_{u,f}$ is the ultimate tensile stress of dry fabric (MPa);
- σ_V is the axial stress of the column (MPa);
- $\sigma_{Vmax,RM}$ is the compressive strength of the confined masonry column (MPa);
- $\sigma_{Vmax,URM}$ is the compressive strength of the unconfined masonry column (MPa).

Abstract

The conservation and the preservation of existing masonry buildings, most of them recognized as cultural heritage, require retrofitting techniques that should reduce the invasiveness and assure reversibility and compatibility with the substrate. In this perspective the strengthening system should be able to improve the bearing capacity of the structural member and, at the same time, to assure mechanical and material compatibility. The use of *Fabric Reinforced Cementitious Matrix* (FRCM) composites is now recognized to be suitable for these purposes. In fact, the inorganic matrix has comparable properties with respect to the existing historical mortars while the fabric has relevant tensile strength. At the same time these systems assure satisfactory level of reversibility (or at least removability). In this scenario, the present research aims to investigate the FRCM-confinement of masonry columns focusing on the influence of specific parameters, still poorly investigated, in order to deeply understand their effect on the mechanical response. In particular, the experimental variables are: the type of masonry substrate (*Tuff* and clay brick with lime-based mortar), the type of FRCM system (glass dry mesh + lime-based mortar and steel mesh + lime-based matrix) and the number of plies (1, 2 and 3). In addition, a detailed experimental characterization of the utilized materials has been carried out, including bond test between the reinforcement and the substrate. The results evidenced that the FRCM is an effective solution for masonry column confinement once a proper design is performed, taking into account all involved parameters. The different strengthening systems exhibited different failure modes. Generally, a single ply of external reinforcement produced a negligible increase of bearing capacity. Both strengthening systems applied with multi-ply strengthening schemes produced a significant increase in terms of strength and ultimate axial deformation. This benefit was observed for both *Tuff* and clay masonry columns.

Two available design-oriented formulas, reported in Italian CNR (*National Research Council*) and ACI (*American Concrete Institute*) guidelines have been utilized, in order to further investigate their availability, mostly in case of multi-layered reinforcement. The performed comparisons highlight that the two design relationships provide similar and accurate results when referred to the GFRCM (*Glass*-FRCM) system in 1- and 2-layers' configurations, while the predictions appear conservative when 3 layers of GFRCM are utilized, for both masonry types. Considering the SRG (*Steel Reinforced Grout*) system the results predicted by the two models are more scattered, mostly when the number of layers increases. In addition, the formulation proposed by CNR appears more accurate in case of *Tuff* masonry while the ACI predictions are closer to the experimental results in the case of clay brick masonry.

Keywords: masonry, FRCM, confinement, design-oriented model, testing, columns.

Introduction

A large number of existing masonry structures requires strengthening or retrofitting solutions due to seismic events, long-term degradation, creep, foundation settlements, construction defects/manipulations, or increased capacity demand due to overloads. The use of fiber-reinforced materials, in place of traditional techniques such as steel ties or reinforced concrete jackets, has been largely investigated in the last decades [1]-[2]. Composite materials made by high-strength fiber sheets embedded within organic matrices, referred to as *Fiber-Reinforced Polymer* (FRP), were extensively used as *Externally Bonded Reinforcement* (EBR) of both existing masonry and concrete structures. A number of experimental and theoretical studies were published in the literature over the years, thus showing the strong interest by the scientific community and industry towards the application of these appealing materials [4]-[12]. FRPs present high strength-to-weight ratio, good durability, and possibility of being *ad hoc* engineered to meet the targeted structural requirements. However, the use of organic adhesives raised some drawbacks when applied to masonry structures. The poor composite-substrate compatibility, the low permeability of the strengthened surface, and the difficulties in removing the FRP sheets without damaging the substrate generated some limits to the applications in this field [13]-[14].

In an attempt to overcome these issues, the organic binder was replaced with an inorganic matrix and the high-strength fiber sheet with a high-strength open-mesh textile. In this way a new type of fiber-reinforced inorganic-matrix composite was proposed, usually referred to as *Fabric Reinforced Cementitious Matrix* (FRCM) [15]-[16] or *Textile Reinforced Mortar* (TRM) [17]. The name *Steel Reinforced Grout* (SRG) is adopted when the textile is made by steel cords [20]-[19]. As in the case of FRPs, FRCMs can be applied as EBR on masonry members and were proven to be effective in increasing both the in-plane and out-of-plane capacity of masonry walls [21]-[22], collapse loads of masonry arches [23], and compressive strength of masonry columns [24]-[30]. FRCMs can be made using different types of fiber (e.g. glass, basalt, carbon, *poliparafenilene benzobisoxazole* – PBO, hemp, flax, and steel in the case of SRG) and different matrices (e.g. lime-based, cement-based, and geopolymers), which combination leads to different physical and mechanical properties of the composite. The main advantages of FRCMs when compared with FRPs consist of high compatibility with poor substrates (i.e. ancient masonry) and satisfactory reversibility of the application. As well known, the last issue is crucial and quite controversial; finding the optimal compromise between safety and conservation is still challenging and some studies have been also focused on the assessment of reversible FRPs strengthening techniques [31].

Due to the different behaviors observed for FRCM composites, research studies were carried out to identify the main parameters that characterize the mechanical response of these materials. In light of available researches, the first recommendations for design were published [15] and [32]. Within the framework of the Rilem Technical Committee 250-CSM (*Composites for the Sustainable strengthening of Masonry*), a *Round Robin Test* (RRT) focused on the tensile response and bond behavior of various FRCMs considering different masonry substrates. The results were useful to provide indications for testing and to gain a better insight into the mechanical performances of each specific material [33]-[40].

Although numerous studies regarding the tensile and bond behavior of FRCM composites can be found in the literature and *Initial Type Testing* (ITT) and design guidelines are currently available, some issues still remain unsolved. Among them, the identification of the contribution of the FRCM-confinement of masonry columns is one of the most debated. Available research indicates that several parameters affect the contribution of the FRCM jacket to the axial capacity of masonry columns. They include the mechanical and geometrical properties of substrate and composite, number of textile layers and matrix thickness, and textile and matrix maximum strain capacity [41]-[44]. Experimental outcomes showed that increasing the number of textile layers may increase the axial strength and deformability of the column [45]. However, this increase is affected by the type of FRCM and by the column cross-section aspect ratio [47]. In some cases, a low number of textile layers may lead to negligible increments of the column axial strength, although the deformation capacity may increase [48]. Therefore, the number of textile layers appears one of the crucial parameters for the reliable evaluation of the strengthening effectiveness. Although analytical models were proposed to predict the behavior of FRCM-confined masonry columns [15], [32] and [42]-[44], further investigations are needed to assess the models accuracy and reliability with respect to different parameters.

In this paper, the results of a RRT campaign on masonry columns made by clay bricks and *Tuff* stone, and confined with different number of layers of either glass FRCM or SRG are presented and discussed. The RRT program was organized within the framework of the ReLUIS-DPC 2019–2021 project (WP 14) funded by the *Italian Department of Civil Protection* and involved 8 universities. The experimental variables investigated are: the type of masonry (clay brick or *Tuff* stone), FRCM type (glass FRCM or SRG), and number of reinforcement layers (from 1 to 3 layers). The obtained results help to gain an insight on the contribution of the FRCM to the axial behavior of confined masonry columns, mostly referring to the influence of the number of layers varying the type of masonry and the reinforcement. In addition, the comparison between experimental results and those predicted by using the two available guidelines, namely CNR-DT215 [32] and ACI 549-R13 [15], are reported and discussed.

Experimental program

The experimental program aimed to investigate the mechanical behavior of masonry columns confined by multi-ply FRCM systems and subjected to uniaxial compressive load. Their application, indeed, often involves the use of multiple layers in order to accomplish design requirements, due to the low fibers density generally characterizing such systems. A RRT was, thus, performed, involving eight Italian laboratories: University of Bologna (*UniBo*), University of Calabria (*UniCal*), University of Firenze (*UniFi*), Polytechnic of Milan (*PoliMi*), University of Naples – Federico II (*UniNa*), University of Salento (*UniSal*), University of Salerno (*UniSa*) and University of Palermo (*UniPa*). Two different types of masonry, commonly adopted in Italy, were used to build the columns, namely clay bricks and *Tuff* stones; in both cases a lime-based mortar was employed as binder, as traditionally made for historical masonry. Moreover, two types of FRCM were used: glass dry mesh and steel wires sheet, both embedded in a lime-based mortar. The two systems will be referred in the following as GFRCM (*Glass Fabric Reinforced Cementitious Mortar*) and SRG (*Steel Reinforced Grout*). For the first FRCM system an adhesion promoter, labeled IPN (*Interpenetrated Polymer Network*), was used according to the manufacturer's instructions, in order to improve the bond between the inorganic matrix and the reinforcing fibers.

Test program, specimens and realization

A total of 64 half-scale column specimens were built: 32 columns (24 confined and 8 unconfined) were prepared at *UniSal*, while 32 columns (28 confined and 4 unconfined) were prepared at *UniBo.* The columns were strengthened by a variable number of reinforcement plies. The experimental work plan is reported in Table 1.

Table 1. Round robin work plan.

Construction laboratory	Testing laboratory	Masonry substrate	FRCM	# ref. column	# 1-ply column	# 2-ply column	# 3-ply column
UniSal	*UniSal*	*Tuff*	GFRCM	2	2	2	2
	UniPa			2	2	2	2
	UniCal	Clay brick		2	2	2	2
	UniNa			2	2	2	2
UniBo	*UniFi*	*Tuff*	SRG	1	3	2	2
	UniSa			1	3	2	2
	UniBol	Clay brick		1	3	2	2
	PoliMi			1	3	2	2

The geometrical dimensions of the specimens are reported in Fig. 1. The bricks had the same dimensions for both types of masonry, i.e. 125x250x55 mm^3, while the horizontal mortar joints thickness was 10 mm and 15 mm for the clay brick and the *Tuff* columns, respectively. A corner radius of 20 mm was realized along the height of the specimens to avoid possible premature failure of the fibers, due to stress concentration at the corners (knife-effect). The rounding of the corners was made for each block, by using a computer aided manufacturing tool in order to minimize the possibility of manpower error.

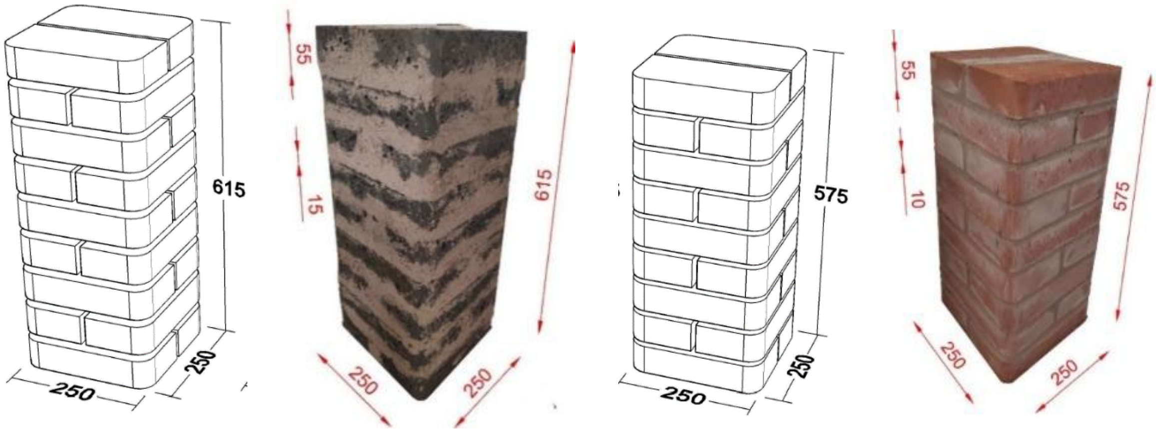

a) *b)*

Fig. 1. Specimens dimensions, in mm. a) Tuff stone and b) clay brick masonry.

The confining system used at *UniSal* consisted of a lime-based mortar and a dry glass mesh; the spacing of the mesh was 12x12 mm, with a 60 mm^2/m equivalent thickness in the two orthogonal directions and a density of 300 g/m^2. The reinforcement used at *UniBo* consisted of a hydraulic lime-based mortar and a sheet of unidirectional steel wires made by high strength galvanized steel cords, with a density of 670 g/m^2 and cross-sectional area of each cord equal to 0.538 mm^2. The steel cords were held together by a glass fiber mesh, to facilitate the installation of the reinforcement.

The FRCM installation's procedure is illustrated in Fig. 2 and Fig. 3. Preliminarily, all the columns surfaces were soaked in order to quasi-saturate the masonry. A first layer of mortar (5 mm thick) was applied; then, the specimens were wrapped by the glass grid/steel sheet with an overlapping length $\geq \frac{1}{4}$ of the perimeter of the cross-section; in particular an overlapping length of 375 mm and 250 mm was adopted for SRG and GFRCM systems, respectively. The mortar was forced to go through the voids of the grid by pressing it with a trowel, for a proper impregnation. For the single layer-reinforcement, the final step consisted in covering the grid, wet-on-wet, with a second layer of mortar (≈5 mm thick). For the 2nd and 3rd mesh layers, the application procedures described above were repeated, achieving a total thickness of 15 mm and 20 mm, respectively. In the case of multi-layers confinement, the overlapping portion for each layer was positioned on different faces of the column, to avoid a weak region in the confinement jacket. In the case of GFRCM, the glass mesh was applied with a single full-height grid around the column, while for SRG two sheets were utilized, each covering half of the column's height, as prescribed by the manufacturer. In addition, the application of the GFRCM system involved the use of an adhesion promoter, IPN-01 type basically aimed at protecting the fibers from the alkaline environment of the mortar and at improving the bond between the mesh and the mortar. It was applied along the lateral surfaces of the columns before and after the positioning of the glass mesh, and activated by the humidity of the mortar. Once realized, specimens were cured for at least 28 days in laboratory conditions and then sent to the other university partners to be tested.

a) *b)* *c)* *d)* *e)*

Fig. 2. GFRCM-confinement phases: a) first mortar layer, b) first layer of IPN-01, c) glass fabric wrapping, d) second layer of IPN-01 and e) second layer of mortar

a) *b)* *c)* *d)*

Fig. 3. SRG-confinement phases: a) clay brick column, b) first layer of mortar, c) steel sheet wrapping, d) second layer of mortar.

Test set-up

Compressive tests were carried out in all the 8 laboratories involved in the research activity by using specifications shared between them and according to the test arrangement shown in Fig. 4.

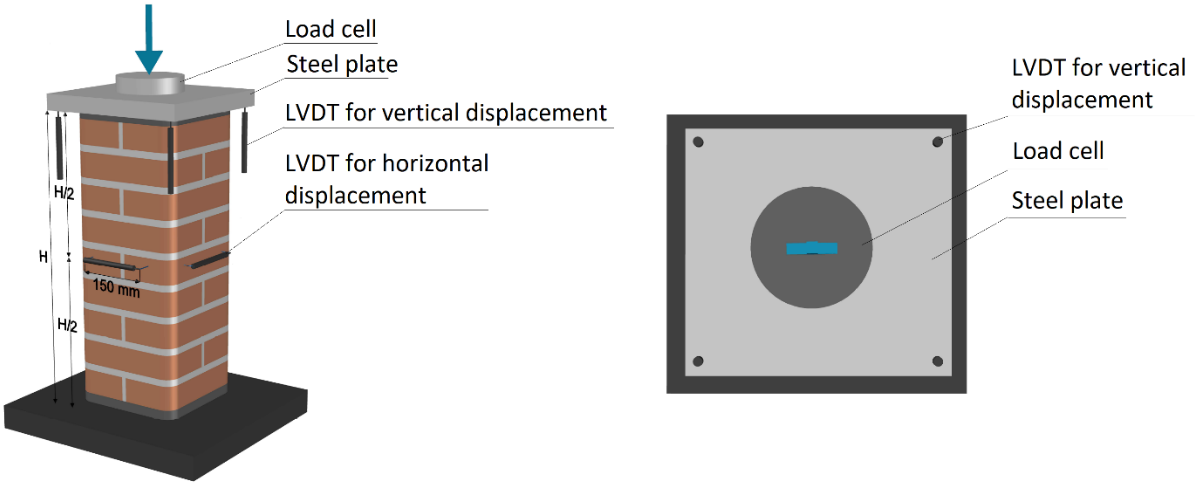

Fig. 4. Scheme of the test set-up.

It has to be noted that, in order to prevent any contact of the FRCM jacket with the steel plate distributing the axial load on the column and, thus, the occurrence of local buckling of the jacket, a small portion at both the top and bottom of the confined specimens, approximately 10 mm high, was always left unconfined.

Although in the present RRT common procedures were agreed and basically respected, slight differences in the test equipment and set-ups were observed and will be discussed in the following (see also Table 2). Most labs used a hydraulic testing machines, the others a hydraulic jack or actuator; moreover, except at the UniBo, UniCal and UniSal, tests were carried out in displacement control at a rate ranging between 0.3 and 0.5 mm/min, up to the failure. In order to detect the post-peak behavior, the softening phase was continued up to a conventional collapse, for tests performed in load control. The latter being generally identified on the softening branch when the measured force was about 80% of the peak load ("conventional collapse"). Horizontal elongation and vertical shortening as well as the axial load were recorded. To measure the formers, most of the laboratories used *Linear Variable Displacement Transducers* (LVDTs), directly connected to the FRCM specimens; in some cases, potentiometers were also used. In particular, four measures were recorded by each lab for both axial shortening and transverse elongation; vertical transducers were often placed at the corners of the specimens, thus allowing for both the measurement of the axial shortenings and the verification of possible load eccentricities during the test. The data acquisition frequency was not the same for all the laboratories but a minimum of 2 Hz was always assured in order to register a sufficient amount of readings. Test results are mainly given in terms of maximum and ultimate load and corresponding vertical and lateral deformations; therefore, the corresponding axial stress-axial strain curves and axial stress-lateral strain responses were obtained and plotted for each tested specimen. Fig. 5 shows some pictures of the various test set-ups.

Some specific remarks characterizing the experimental program should be taken into consideration; they are listed in the following:

- in some labs, the unconfined masonry specimens were weighted before testing in order to obtain the actual mass density; *Tuff* and brick-based masonry specimens were characterized by a mass density equal to about 14 kg/m^3 and 16 kg/m^3, respectively.

- When the end surfaces were not perfectly parallel, a capping with a layer of high-strength mortar or similar material was applied at both the bottom and the top of the columns (this is the case of the Universities of Bologna, Naples and Palermo for confined columns) or only at the top (this is the case of the University of Florence and Palermo for all the specimens and just for the unconfined columns, respectively) as shown in Fig. 6.
- In some cases, low-level load cycles were performed before starting the test in order to check the experimental set-up. In particular, the Universities of Bologna, Naples, Palermo and the Polytechnic of Milan performed cycles between 40 and 50 kN before starting with the monotonic increase of the axial displacement up to collapse.

Table 2. Description of the test set-up per laboratory.

Lab	Testing machine	Measuring tools for Load	Measuring tools for Axial Displacements	Measuring tools for Horizontal Displacements	Test performed in	Rate
UniBo	Hydraulic universal testing machine (60 kN capacity)	Pressure transducer (5 bar)	4 LVDTs with a recording length of 50 mm	4 LVDTs with a recording length of 20 mm applied at mid-height (gauge length 150mm)	Load control	4 N/s
UniCal	Hydraulic jack	External load cell of (10 KN)	4 LVDTs	4 LVDTs with a gauge length equal to 150 mm	Load control	40 N/s
UniFi	Hydraulic press (3 tons full-scale)	Resistance load cell (2 tons full-scale)	4 resistance displacement transducers (full-scale 1mm)	4 P-shape resistance displacement transducers (full-scale ± 5mm, allowed gauge length from 1 to 150 mm, used gauge length 150 mm)	Displacement control	0.4 mm/min (up to the conventional ultimate load) 1 mm/min from such ultimate load to the end of test
UniSal	Hydraulic Jack	External load cell (30 tons)	4 LVDTs with a gauge length of 1 mm	4 LVDTs applied at mid-height (gauge length 150mm)	Load control	Not controlled
PoliMi	Servo-hydraulic universal testing machine with 25 kN capacity	25 kN load cell	4 LVDTs	4 LVDTs with a gauge length of approximately 2 mm	Displacement control	0.2 mm/min
UniNa	Hydraulic actuator with load capacity of 25 kN in tension and 30 kN in compressive	External 10 kN load cell	4 LVDTs	4 LVDTs with a gauge length of 150 mm placed in the midpoint	Displacement control	0.4 mm/min
UniPa	Universal testing machine with load bearing capacity equal to 40 kN	Pressure transducer integrated in the testing machine, according to a prior calibration with external load cell	4 Linear Variable Displacement Transducers (LVDTS)	4 LVDTs having a gauge length of 150 mm	Displacement control	0.3 mm/min
UniSa	Hydraulic actuator with load capacity of 30 kN in compressive and 25 kN in tension	Load cell integrated in the testing machine	4 Potentiometers (gauge length 3 mm)	4 Potentiometers applied at mid-height (gauge length 150 mm)	Displacement control	0.3 mm/min

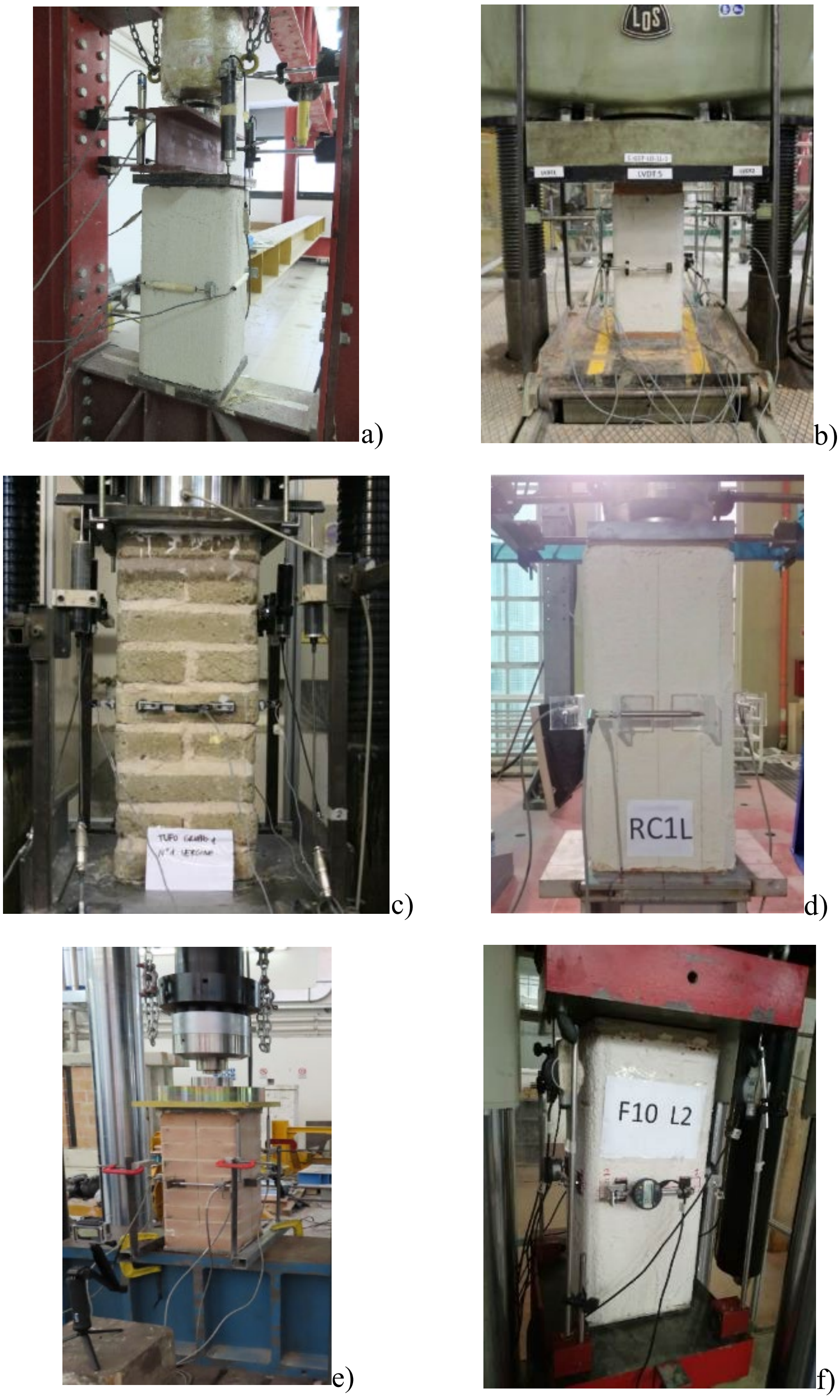
a)
b)
c)
RC1L
d)
F10 L2
e)
f)


g)

h)

Fig. 5. Test setup - a) UniSal; b) UniBo; c) UniFi; d) UniCal; e) UniNa; f) UniPa; g) UniSa; h) PoliMi.

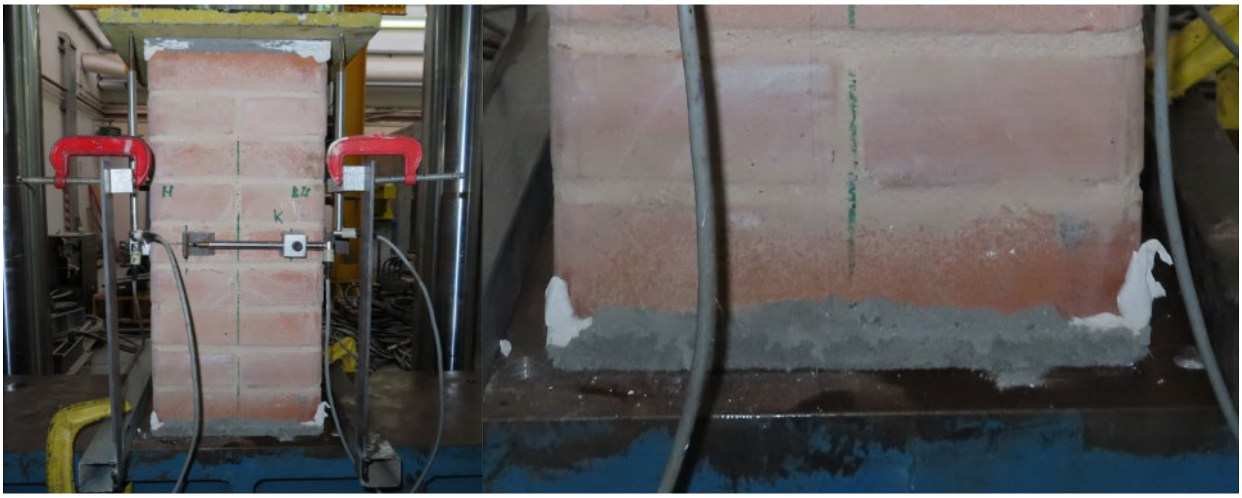

Fig. 6. Mortar layers placed on top and bottom face of masonry specimens (UniNa).

Materials and Bond properties

The present section describes the tests realized for the mechanical characterization of all utilized materials. Half of the characterization was carried out by *UniSal* and the other half by *UniBo*. The mortar used in masonry joints was tested according to EN standard [49], while the compressive strength of bricks was obtained according to [50]. In particular, a number of 30 specimens was tested for mortar. Ten cylindrical samples with equal height and diameter (50 mm for clay bricks and 105 mm for *Tuff*) were tested for bricks. The experimental investigation also included uniaxial compressive tests on three stacked bricks masonry prisms [51]. The average compressive strength, $f_{c,m}$, for all the tested materials are reported in Table 3.

Table 3. Compressive tests results

Material	**$f_{c,m}$ (*UniSal*) (MPa)**	**$f_{c,m}$ (*UniBo*) (MPa)**
Mortar (masonry joints)	4.35 (Co.V.=0.05)	5.71 (Co.V.=0.06)
Clay brick	24.06 (Co.V.=0.14)	19.33 (Co.V.=0.08)
Tuff stone	5.26 (Co.V.=0.34)	5.67 (Co.V.=0.28)
Clay brick masonry prism	5.16 (Co.V.=0.15)	6.21 (Co.V.=0.07)
Tuff masonry prism	2.17 (Co.V.=0.20)	3.19 (Co.V.=0.10)

Regarding the GFRCM and SRG reinforcement, several specimens were prepared and tested under direct tensile conditions, according to [52]. A total of nine GFRCM specimens were tested, sized 6x60x10 mm^3 and including four longitudinal yarns of fabric spaced 12 mm (with an adhesion promoter IPN-01 type at fabric/mortar interface); twenty SRG specimens were also tested, sized 4x40x10mm^3, including five longitudinal steel cords spaced 6.35 mm. The tensile strength, the elastic modulus and the maximum elongation obtained from tests are reported in Table 4. For FRCM coupons, the reported elastic moduli E_1 and E_2 correspond to the slope of the first and of the second branch of the stress-strain curve, respectively. The tensile strength was computed as the ratio between the peak load and the cross-section of the dry fabric.

The average tensile stress-strain curves of the composites systems (GFRCM and SRG) are reported in Fig. 7, overlapped with the stress-strain curves of the corresponding dry fabric/sheet. Fig. 7*a* refers to GFRCMs, where the constitutive law is characterized by a bi-linear curve with a transition curve in between. The ultimate slope is slightly lower when compared to that of the dry fabric, while a significant reduction of the maximum deformation and strength was registered. This result is caused by the uneven stress distribution within the fibers after the matrix cracking that involved a premature failure of the most loaded yarns. Fig. 7b shows the stress-strain curve for the SRG-system. In this case, the composite exhibited an almost tri-linear behavior with a third branch more predominant with respect to the other two. The ultimate strength of the dry steel fabric was comparable to that of the SRG; also, the scatter between the elastic modulus of the fabric and the slope of the third branch of the stress-strain curve of SRG specimens appears negligible, while the ultimate deformation of the SRG is slightly lower if compared with that of the dry fabric.

Table 4. Tensile test results.

Component tested	$\sigma_{u,f}$ (MPa)	σ_u (MPa)	E_1 (GPa)	E_f (GPa)	E_2 (GPa)	$\varepsilon_{u,f}$ (%)	ε_u (%)
Glass mesh	1929 (CoV=0.14)	-	-	108.0 (CoV=0.16)		1.80 (CoV=0.12)	
GFRCM coupons	-	891 (CoV=0.15)	514.5 (CoV=0.08)	-	77.5 (CoV=0.05)	-	0.97 (CoV=0.19)
Steel sheet	3080 (CoV=0.04)		-	193.4 (CoV=0.10)		2.17 (CoV=0.11)	
SRG coupons	-	2972 (CoV=0.03)	1243.6 (CoV=0.13)	-	197.4 (CoV=0.10)	-	1.86 (CoV=0.12)

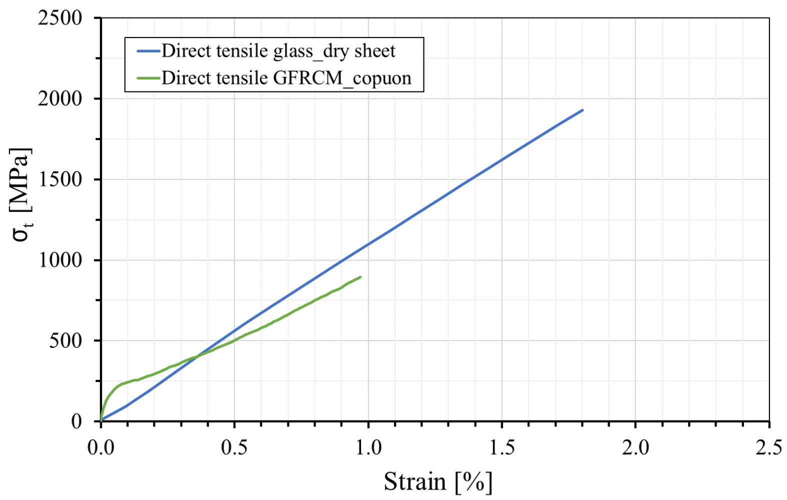

a)

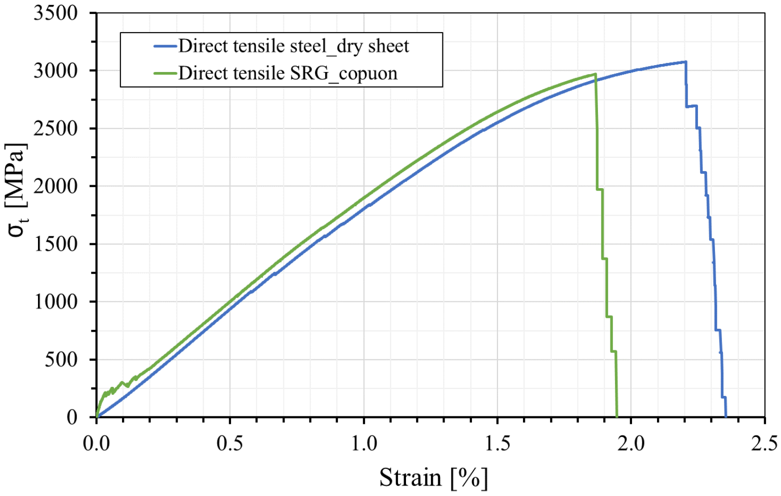

b)

Fig. 7. Comparison between the tensile behavior of the dry fabric and that of the inorganic based composite: a) GFRCM and b) SRG.

The matrix (mortars) of the two composite typologies were tested after 28 days curing to evaluate their compressive strength, according to [49]; it resulted equal to 9.1 MPa (CoV=0.27) for GFRCM, and 13.4 MPa (CoV=0.09) for SRG. Single lap shear tests were also performed in a recognized set-up, described in [35]-[39], by using the two considered masonry substrates: clay bricks and *Tuff* stones. Specimens dimensions are represented in Fig. 8; the composite strip was applied to the long faces of the clay bricks and to the short faces of the *Tuff* stones, as indicated in [53] and shown in Fig. 8. Tests were carried out under displacement control with a load rate of 0.2 mm/min. A total of 10 specimens were tested per each substrate.

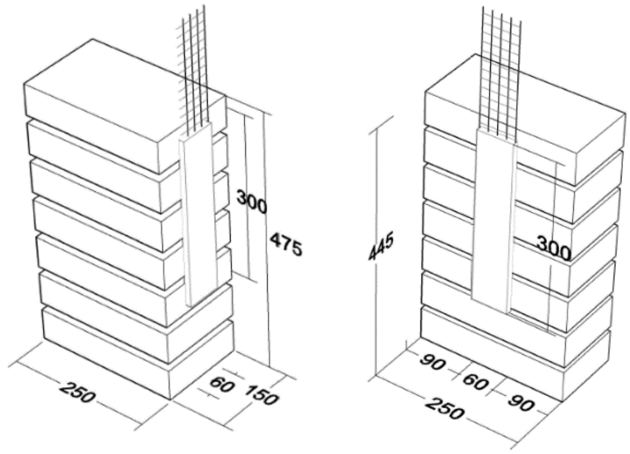

a) *b)*

Fig. 8. Bond test specimens: a) Tuff substrate, b) clay bricks substrate.

In Table 5 the values of the limit bond stress, $\sigma_{lim,b}$, , the conventional limit stress, $\sigma_{lim,conv}$, assumed equal to the mean value of the $\sigma_{lim,b}$ the corresponding deformation, $\varepsilon_{lim,conv}$ and the ratio between $\sigma_{lim,conv}$ and $\sigma_{u,f}$ are reported. According to the CNR DT 215 [32], the limit bond stress is evaluated dividing the maximum bond load (F_{max}) by the cross-section of the dry fabric (A_f), while the conventional limit deformation is obtained dividing $\sigma_{lim,conv}$ by E_f, namely the mean value of the *Young's modulus* of the fabric.

Table 5. Single lap shear test results.

Lab	***FRCM type***	***Substrate***	***Failure mode****	F_{max} (*kN*)	*s* (*mm*)	$\sigma_{lim,b}$ (F_{max}/A_f) (*MPa*)	$\varepsilon_{lim,conv}$ (%)	$\sigma_{lim,conv}/\sigma_{u,f}$ (%)
UniSal	***GFRCM***	*Tuff*	D	1.96	3.97	889.35	0.74	42
			D	2.21	3.76	16.77		
			E - F	0.97	6.52	439.89		
			E	1.89	1.48	859.39		
			E	1.96	0.86	890.10		
			B + E + A	2.09	0.54	949.29		
			E	1.54	0.83	699.84		
			B + E + A	1.51	0.52	685.21		
		(Av.)		1.77	2.31	802.48		
		CoV		23%	95%	23%		
		Clay	E	1.72	1.33	781.90	0.78	44
			B + E + A	1.71	1.20	778.37		
			D	1.96	3.97	889.35		
			B + E	2.03	4.18	923.29		
			B + E	2.04	8.49	929.02		
			E	2.	0.44	910.39		
			D	1.68	0.90	765.79		
			E + F	1.79	7.16	813.76		
			D	1.53	1.21	694.24		
			D	2.	2.36	906.85		
		(Av.)		1.85	3.12	839.30		
		CoV		10%	89%	10%		
UniBo	***SRG***	*Tuff*	B	8.17	2.86	1899.03	0.78	49
			B	7.03	1.76	1632.88		
			B	6.03	1.78	14.02		
			B	6.51	2.34	1511.93		
			B	4.76	1.87	1105.95		
		(Av.)		6.50	2.12	1509.96		
		CoV		19%	22%	19%		
		Clay	B	4.94	1.25	1148.2	0.60	38
			B	4.69	1.25	1090.4		
			B	4.31	1.41	10.6		
			B	6.43	1.86	1494.2		
			B	4.77	1.49	1109.3		
		(Av.)		5.03	1.45	1168.55		
		CoV		16%	17%	16%		

*according to [32]:

- A is the debonding at the matrix-substrate interface
- B is the debonding at the textile-to-matrix interface;

- D is the tensile rupture of the textile (out of the bonded area);
- E is the textile slippage within the matrix with cracking of the outer layer of mortar;
- F is the textile slippage within the mortar matrix.

The failure modes for the GFRCM specimens occurred at the reinforcement to-substrate interface (type A), between the textile and the matrix (type B), or by textile slippage within the matrix (type E and F). Relevant was also the case of fabric rupture (type D) which involved part of the fibers cross-section. The failure often was accompanied by micro-cracks within the matrix, at the interface between the fiber and the matrix or the matrix and the substrate. Finally, the rupture of the fabric in the free zone was also observed. For the SRG specimens, the failure occurred due to the debonding at the textile-to-matrix interface (type B) in all cases.

For GFRCM, obtained $\sigma_{lim,conv}/\sigma_u$ revealed that the tensile strength of the composite system was almost reached in all the tests, independently on the failure mode and on the type of substrate. On the other hand, for SRG the conventional limit strength was significantly lower than the ultimate tensile strength of the composite system, due to the premature bond failures.

Experimental results

Experimental results achieved from monotonic compressive tests were post-processed considering the same assumptions for all the samples. In particular, the performances achieved on Un-Reinforced Masonry (URM) specimens will be used by considering that the columns were manufactured by different research units. Namely, URM columns and specimens strengthened with SRG (clay and *Tuff* masonry), were assembled at UniBo, while those strengthened with GFRCM (clay and *Tuff* masonry) were assembled at UniSal. Raw materials were provided by the same suppliers.

The assumptions made to elaborate the key experimental results were as follow:

- the axial shortening was calculated as the average of the four vertical LVDT readings (Fig. 4). The axial strain was evaluated dividing the axial displacements by the gauge length of the LVDT devices;
- the axial load P, acquired by the load cell transducer (Fig. 4), and the nominal sizes of the masonry cross-section (250x250 mm^2) were used to evaluate the axial stress, σ_V;
- the axial stress-longitudinal strain curves were stopped according to a capacity reduction in the softening phase of about 20%; for the case of hardening behavior, the ultimate value of axial strain was considered in correspondence of the maximum stress;
- the elastic modulus was calculated by evaluating the slope of the axial stress-longitudinal strain curve from the 5% to 40% of the maximum axial stress, σ_V;
- the first axial cracking load, P_{cr} was assessed in correspondence of the first crack directly detected on the lateral surface of the specimen or by the discontinuity detected on the load *vs* displacement curves, at the end of the first almost linear branch. The second approach resulted more reliable for confined columns where the external masonry surfaces were totally covered;
- the hoop elongation/strains were evaluated by considering the average measure obtained from the four horizontal LVDT devices. The lateral measurements provided reliable results from null axial stress up to the first axial cracking load. The hoop strains measured after the formation of the first crack were often jeopardized by the detachment of the LVDT devices, due to cracking of the matrix;
- the increase in load carrying capacity was calculated as the ratio between the maximum stresses recorded for the confined specimens and that for the URM specimens. The latter being the average strength evaluated for unconfined columns made by the same manufacturer; thus, two average values were determined for each kind of masonry (referring to columns realized at UniSal and UniBo). This was considered the most rational choice in order to exclude from the elaboration stage the possible variability typically related to the hand manufacturing process, as better reported in the following. In this context, it should be mentioned that UniBo built two URM specimens for each masonry type (clay brick and *Tuff*), while UniSal built four URM columns for each masonry type.

Unreinforced Tuff masonry

Fig. 9 a-d shows representative cracks and damage patterns for URM specimens tested in the different laboratories.

a)

b)

c)

d)

Fig. 9. Unreinforced Tuff masonry specimens after testing: a) 1_URM UniPa; b) 2_URM UniSal; c) 1_URM UniFi; d) 1_URM UniSa.

The failure modes were always brittle and almost similar in all cases, with several vertical cracks starting from the *Tuff* units and developing also within the mortar joints. Cracks intensified along the middle part of the specimens up to the compressive crushing of the brick units occurred; in some cases, a significant damage was recorded also near the bottom base (Fig. 9a, b, c).

The compressive behavior of URM columns proved to be characterized by a load carrying capacity with high dispersion and a limited softening post-peak response (Fig. 10). However, the average values resulted compatible with the compressive strength of typical *Tuff* masonries and the expected variability caused by that of constituent materials (see Table 3) and by the different hand manufacturing. Fig. 10 shows the compressive axial stress as a function of the vertical and hoop strains for all the *Tuff* URM samples experimentally tested. Curves are differently colored on the basis of the laboratory which performed the tests, while the solid or dotted line refers to the different sets of samples, selected on the basis of the manufacturing place: UniPa and UniSal belongs to the same set, being manufactured by UniSal, while UniFi and UniSa belongs to another set manufactured by UniBo.

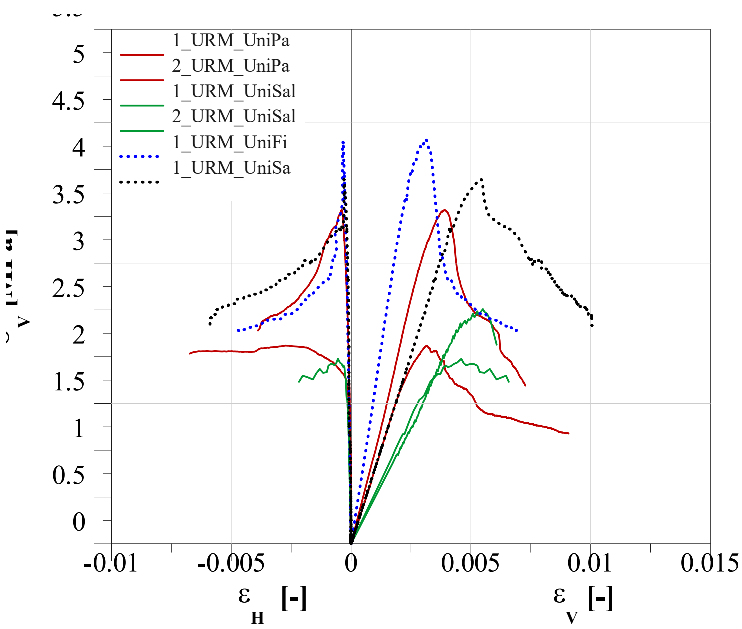

Fig. 10. Axial stress vs. axial and hoop strain for unreinforced Tuff masonry specimens.

The trend of the curves reflects the observed evolution of cracks and damage of the URM specimens. The initial linear trend is followed by a limited non-linear ascending branch after first cracking and up to the soon-reached peak load. The softening post peak phase is characterized by an initial almost-linear branch followed by a curvilinear behavior, corresponding to the extensive cracking stage of the specimen. The mean compressive strength of specimens tested by UniPa and UniSal was equal to 2.54 MPa and the corresponding axial strain was equal to 0.43, while the conventional ultimate strain resulted 0.55. It is worth noting that the URM samples tested by UniFi and UniSa showed a greater average compressive strength (4.11 MPa), but with values of strain at peak and of ultimate strain similar to those evaluated by UniPa and UniSal.

Significant scatters were observed for the measured compressive strengths, being the latter between 1.98 MPa and 3.57 MPa for specimens built in Lecce and tested by UniPa and UniSal, while it was in the range between 3.89 and 4.33 MPa for columns tested by UniFi and UniSa. Differences were obtained also on the measured value of the elastic modulus in compression. The elastic modulus obtained from the tests performed by UniPa was 70% greater than that measured by UniSal; similarly, UniFi obtained a modulus equal to about twice that recorded at UniSa. These differences can be ascribed partially to the different test set-up and partially to the before mentioned variability of the masonry material.

It is also worth noting that the trend of the hoop strains allowed detecting the first cracking load, as the load value for which the hoop strains curves changed the slope suddenly. The corresponding force values were approximately 60% and 80% of the corresponding peak loads, respectively for specimens tested by UniPa and UniSal and by UniFi and UniSa. The experimental results are shown in Table 6, referring to the single specimen and the average values (Av.).

Table 6. Experimental results for unreinforced Tuff masonry.

Outputs	UniPa		UniSal		UniFi	UniSa
	1_URM	2_URM	1_URM	2_URM	1_URM	1_URM
Maximum stress [MPa]	2.12	3.57	2.51	1.98	4.33	3.89
(Av.)	**(2.54)**				**(4.11)**	
Maximum axial strain [-]	0.32	0.39	0.55	0.46	0.31	0.54
(Av.)	**(0.43)**				**(0.43)**	
Ultimate stress [MPa]	1.68	2.87	2.13	1.73	3.42	3.11
(Av.)	**(2.10)**				**(3.27)**	
Ultimate axial strain [-]	0.46	0.45	0.61	0.66	0.36	0.37
(Av.)	**(0.55)**				**(0.37)**	
Maximum hoop strain [-]	0.27	0.04	-	0.05	0.03	0.13
(Av.)	**(0.12)**				**(0.08)**	
First cracking stress [MPa]	1.44	2.40	1.23	1.17	3.69	3.18
(Av.)	**(1.56)**				**(3.44)**	
Elastic modulus [MPa]	798	987	493	540	1658	805
(Av.)	**(705)**				**(1232)**	

Tuff masonry confined by Glass Textile Reinforced Mortar (GFRCM)

Fig. 11 shows some representative specimens confined by the GFRCM system after the tests.

Specimens tested by UniPa *Specimens tested by UniSal*

One layer GFRCM

Two layers

GFRCM

Three layers

GFRCM

Fig. 11. Failure mode of Tuff masonry specimens confined by GFRCM.

The observed failure mode was similar for all the specimens, with the formation of one main critical crack in correspondence of the edge at one corner of the column, starting from the bottom base and developing along the loading direction. This failure mode indicates, as expected, that the stress concentration at the corners, anticipates the tensile failure elsewhere, in the fibres. The tensile breakage of the glass fiber yarns was visible inside the crack, more clearly detectable for specimens confined with one layer of textile; in some cases, the slippage of the fiber from the matrix was also identified by observing a small portion of fiber filaments inside the crack. As expected, the opening of the critical crack was smaller for specimens confined with more layers and larger for one-layer confined specimens.

Tests highlighted the higher confinement efficiency of the multi-ply configuration schemes, as expected. Fig. 12 shows the trend of the compressive strength recorded during the test ($\sigma_{Vmax,RM}$) together with its increase (dimensionless load carrying capacity), being the latter evaluated as the ratio between $\sigma_{Vmax,RM}$ and the average maximum stress for the URM specimens tested by UniPa and UniSal ($\sigma_{Vmax,URM}$). The experimental trend proved to be similar for the two series of samples and independent from the testing laboratory, highlighting the reliability and the repeatability of the tests. In particular, the average maximum stress of the specimens reinforced with one layer of GFRCM proved to be almost similar to the axial capacity of URM samples, meaning that the strength increase due to one-layer of glass FRCM was almost negligible; this is mainly due to the low density of fibrous reinforcement typically used in FRCM systems in relation to the significant lateral expansion of the substrate. Substantial increase of the axial capacity was observed for specimens wrapped with two and three layers. The average strength increase recorded by UniPa and UniSal were equal to 23% and 45% for two layers and 70% and 83% for three layers, respectively.

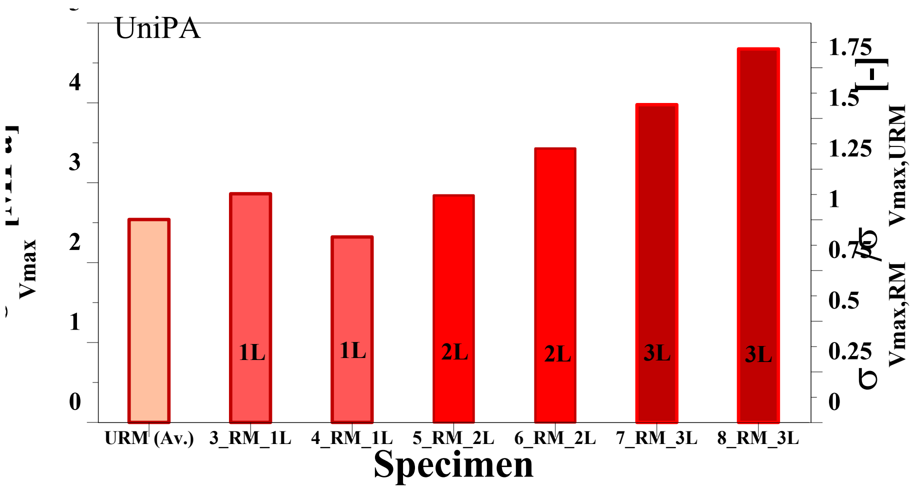

a)

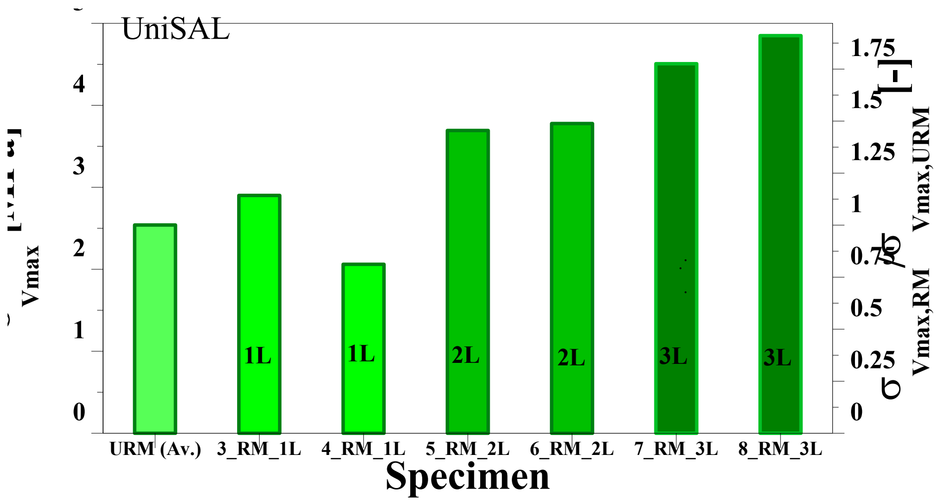

b)

Fig. 12. Maximum stress and dimensionless load carrying capacity of Tuff masonry columns confined by GFRCM: a) specimens tested by UniPa; b) Specimens tested by UniSal

The axial stress *vs* axial and hoop strains (compressive behavior) of the *Tuff* masonry columns confined by GFRCM is reported in Fig. 13 for all the tested columns. In general, a non-linear ascending branch can be observed up to the peak stress, followed by a load drop. This loss of capacity after the peak stress corresponds physically to the compressive crushing of the inner masonry and it is generally followed by a softening branch, which is governed by the behavior of the damaged masonry inside the jacket. Exception is made for the specimens confined with three layers tested by UniSal, which showed a limited load recovery before the failure occurred. The extension of the post-peak branch depended on the number of applied textile layers. Specimens confined with two and three layers of textile exhibited greater strength increases but, in some cases, lower values of ultimate strain (more brittle behavior). The increase of the value of axial strain corresponding to peak stress was equal to 56% for confinement with one and two layers, while it was equal to 18% for specimens confined with three layers, considering the specimens tested by UniPa; the same quantities evaluated for specimens tested at UniSal were equal to 120%, 1% and 156% for confinement with one layer, two and three layers, respectively.

It was also observed that hoop strains were negligible up to the first cracking stress, and increased rapidly afterwards; this confirms that confinement activates after the tensile strain of the masonry is reached. Hoop strains were larger for specimens confined with more layers, showing the ability of a stiffer jacket to carry a greater amount of hoop tensile force and consequently to provide greater values of confinement pressure, as expected.

It is worth noting that the two laboratories performed the tests with a different control, as described in the previous section. UniPa adopted displacement control, while UniSal performed tests under force control. Consequently, the measures of the strains in the post peak branch are different.

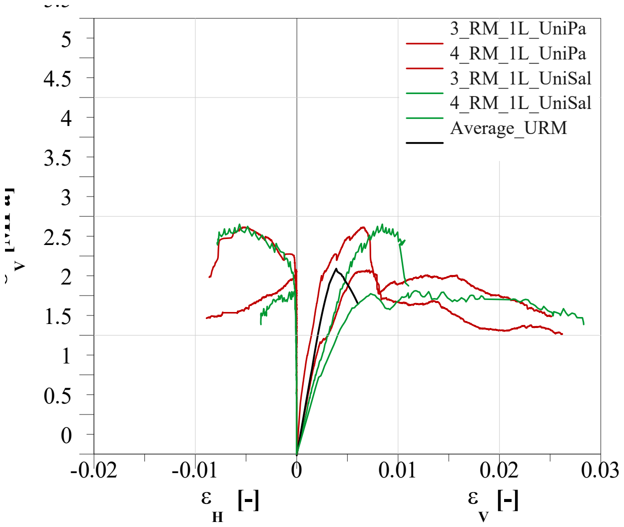

a)

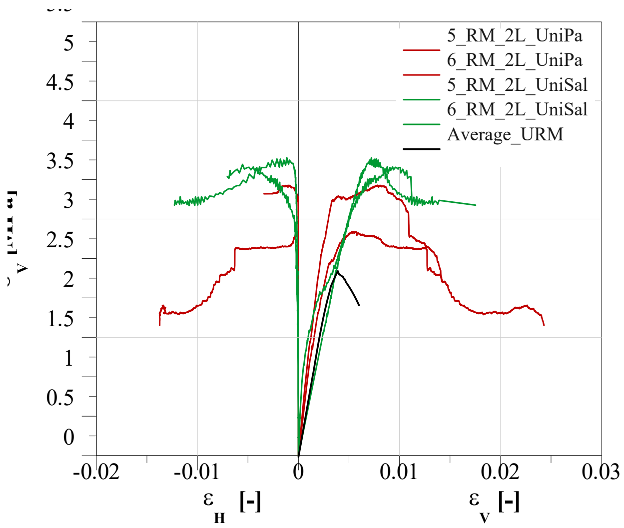

b)

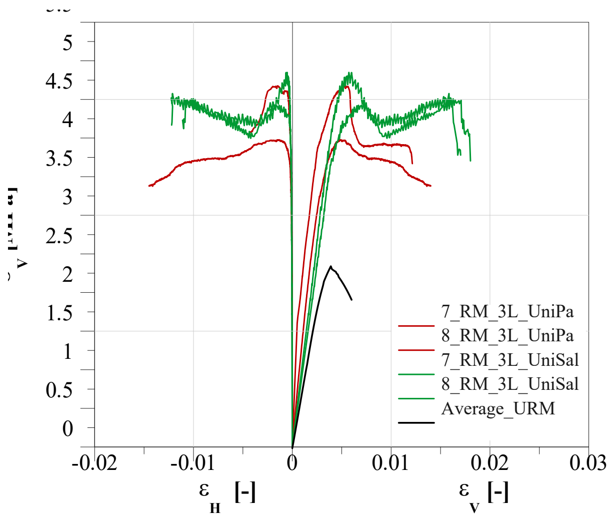

c)

Fig. 13. Axial stress vs. axial and hoop strain for Tuff masonry specimens confined by GFRCM systems. a) Specimens confined with one layer; b) Specimens confined with two layers; c) Specimens confined with three layers.

The experimental results of *Tuff* masonry columns wrapped by GFRCM system are shown in Table 7.

Table 7. Experimental results for Tuff masonry columns strengthened by means of GFRCM systems

Outputs	***Tuff***											
	1 layer				**2 layers**				**3 layers**			
	UniPa		**UniSal**		**UniPa**		**UniSal**		**UniPa**		**UniSal**	
	3_RM	4_RM	3_RM	4_RM	5_RM	6_RM	5_RM	6_RM	7_RM	8_RM	7_RM	8_RM
Max. stress [MPa]	2.86	2.32	2.90	2.06	2.84	3.43	3.69	3.78	3.98	4.68	4.51	4.85
(Av.)	(2.59)		(2.48)		(3.14)		(3.74)		(4.33)		(4.68)	
Max. axial strain [-]	0.65	0.69	0.84	0.0117	0.55	0.78	0.0101	0.72	0.48	0.53	0.0163	0.57
(Av.)	(0.67)		(0.0101)		(0.67)		(0.87)		(0.51)		(0.0110)	
Ultimate stress [MPa]	2.32	1.86	2.64	1.66	2.28	2.74	3.24	3.18	3.38	3.74	3.60	3.86
(Av.)	(2.09)		(2.15)		(2.51)		(3.21)		(3.56)		(3.73)	
Ultimate axial strain [-]	0.75	0.0227	0.0101	0.0283	0.0141	0.0116	0.0112	0.0175	0.0140	0.0121	0.0190	0.0169
(Av.)	(0.0151)		(0.0192)		(0.0129)		(0.0144)		(0.0131)		(0.0179)	
Max. hoop strain [-]	0.51	0.2	0.56	0.02	0.01	0.09	0.55	0.12	0.13	0.15	0.0102	0.052
(Av.)	(0.26)		(0.29)		(0.05)		(0.34)		(0.14)		(0.54)	
First cracking stress [MPa]	1.01	1.36	1.18	0.99	1.35	1.30	0.55	2.49	3.09	1.60	3.65	3.26
(Av.)	(1.18)		(1.09)		(1.32)		(1.52)		(2.35)		(3.46)	
Elastic modulus [MPa]	1469	668	541	449	1082	1326	2586	632	1331	2855	939	1051
(Av.)	(1068)		(495)		(1204)		(1609)		(2093)		(995)	
$\sigma_{Vmax,RM}/\sigma_{Vmax,URM}$	1.13	0.91	1.14	0.81	1.12	1.35	1.45	1.48	1.56	1.84	1.77	1.91

Tuff masonry columns confined by SRG

The failure modes of specimens confined by SRG were substantially different from those observed for GFRCM confined specimens, as expected, and they are reported in Fig. 14. Initially, compressive crushing damage appeared into the upper part of the columns, which was not wrapped by the external jacket. Subsequently, several vertical cracks formed along the external SRG jacket, mainly in correspondence of the edges and near the upper part of the specimen. After extensive cracking, a prominent vertical crack appeared on the SRG jacket at the top or bottom ends of the column, followed by the detachment of the overlapped part of the jacket. In addition, an apparent horizontal crack occurred at mid height of the specimen, together with further horizontal cracks in the upper part; they were generally followed by the spalling of the matrix, as shown in Fig. 14. For specimens confined with more layers, compressive crushing was observed also at the bottom of the specimens.

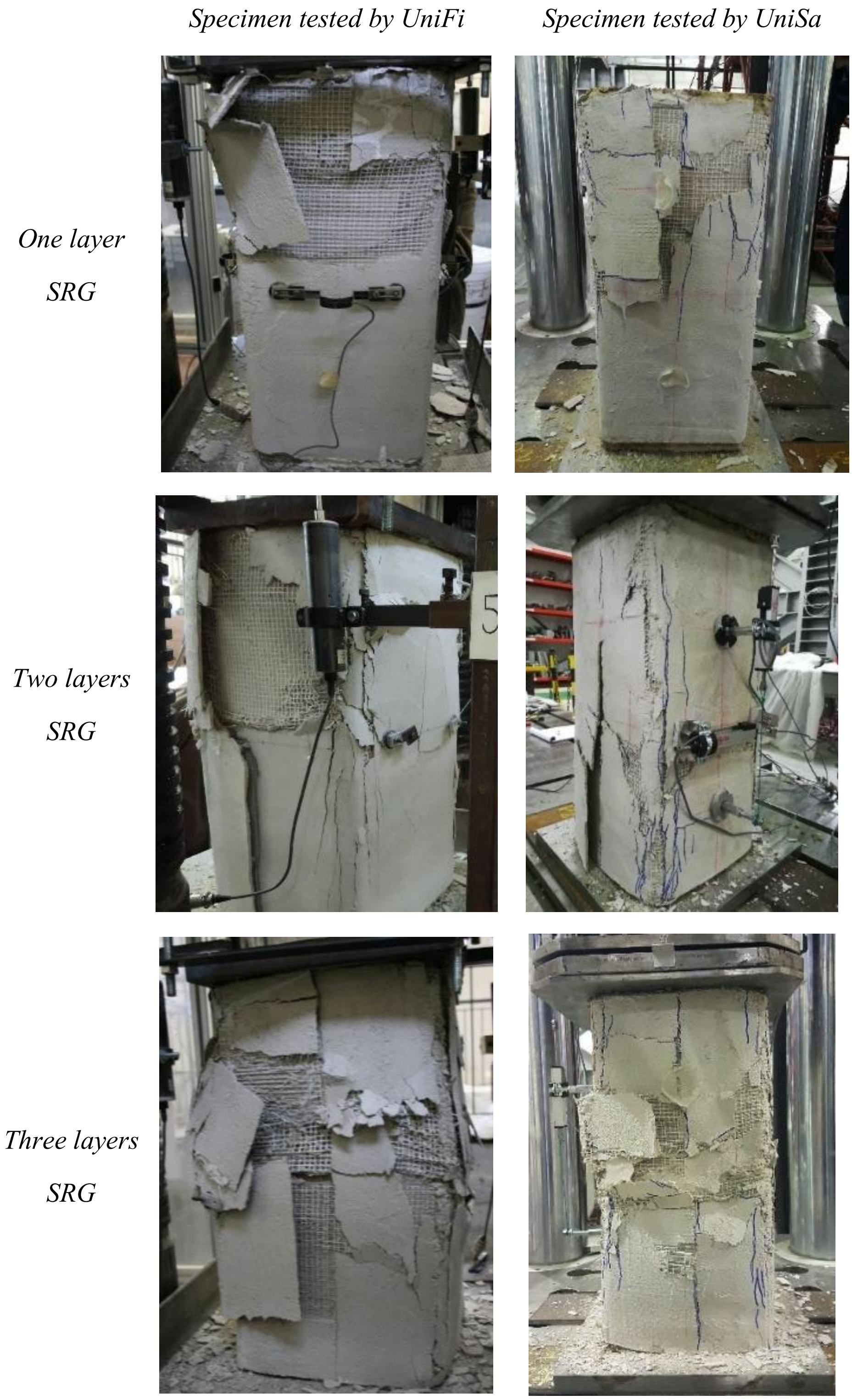

Fig. 14. Failure mode of Tuff masonry specimens confined by SRG.

Fig. 15 shows the maximum axial stress $\sigma_{Vmax,RM}$ recorded during the test and the increase in load carrying capacity for *Tuff* masonry specimens wrapped by SRG. The latter was evaluated as the ratio between $\sigma_{Vmax,RM}$ and the average maximum stress, $\sigma_{Vmax,URM}$ recorded in the two unreinforced columns tested by UniFi and UniSa. The specimens wrapped by one layer had a limited average strength increase, equal to 10% for UniFi and 21% for UniSa. More consistent enhancements were observed for specimens reinforced with two and three layers. In particular, strength increase for samples tested at UniFi was equal to 30% and 33% for two and three layers, while the corresponding values for columns tested at UniSa were equal to 40% and 52%, respectively.

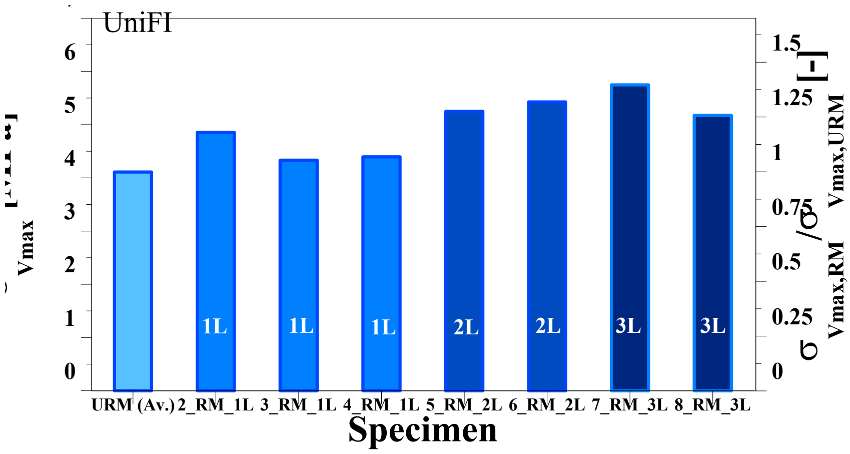

a)

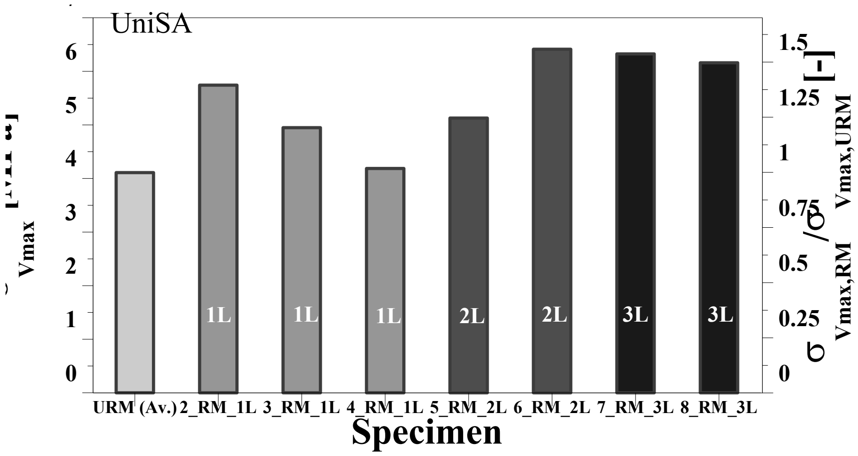

b)

Fig. 15. Maximum stress and dimensionless load carrying capacity of Tuff masonry columns confined by SRG a) Specimens tested by UniFi; b) Specimens tested by UniSa.

It should be observed that the effect of SRG confinement is different from that detected for GFRCM; in fact, the latter produced a higher increase of strength while for the former a significant increase of the deformation capacity was registered.

The trend of the axial stress as a function of axial and hoop strains for SRG confined *Tuff* masonry columns is reported in Fig. 16. The trend of these curves is initially linear up to the stress corresponding to first cracking. This branch is followed by a load drop, in correspondence of the masonry crushing near the column ends. The post-peak branch appeared to be dependent on the number of adopted layers of steel mesh. In particular, a softening behavior, with a quick load drop, was shown by specimens confined with one layer, while a more "ductile" behavior was recorded for specimens reinforced with two and three layers. The irregular trend of the post-peak branch is connected with the extensive damage of the external jacket and masonry core, characterized by diffuse cracking, slippage of the fabric and spalling of the matrix, in addition to the cracking of the masonry core. It is remarkable that the ratio between the average value of axial strain at peak of confined and unconfined columns, was equal to 14.3 and 16.8, for specimens tested by UniFi, respectively with two and three layers. Concerning the samples tested at UniSa, the same ratios were equal to 7.3 and 20.4, confirming that SRG confinement induces significant increments of deformation capacity, which could be interpreted as pseudo-ductility.

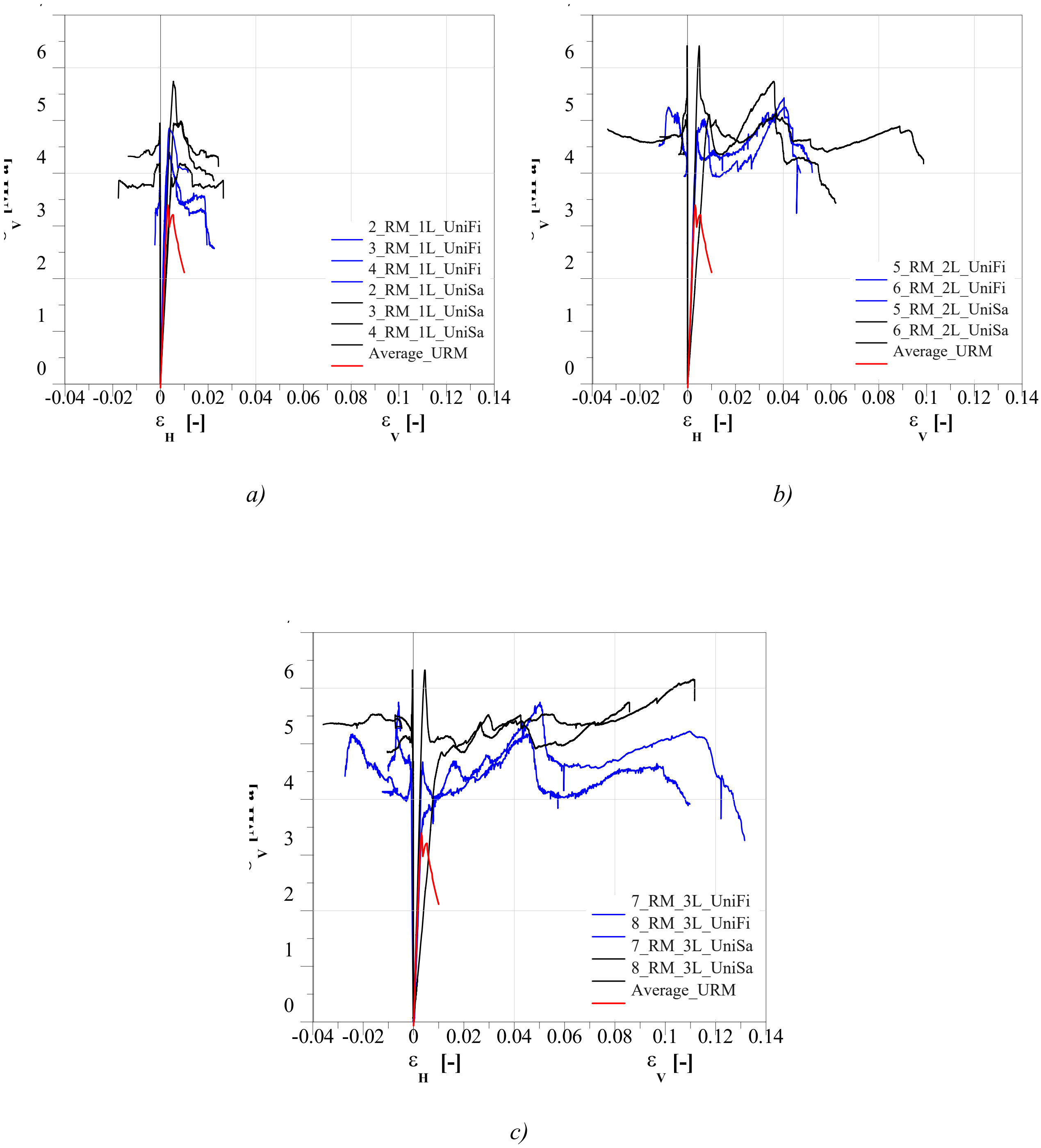

Fig. 16. Axial stress vs. axial and hoop strain for Tuff masonry specimens confined by SRG. a) Specimens confined with one layer; b) Specimens confined with two layers; c) Specimens confined with three layers.

Results recorded from tests on *Tuff* columns strengthened by SRG are reported in Table 8.

Table 8. Experimental results for Tuff masonry columns strengthened by means of SRG systems.

Outputs	***Tuff***													
	1 layer						**2 layers**				**3 layers**			
	UniFi			**UniSa**			**UniFi**		**UniSa**		**UniFi**		**UniSa**	
	2_RM	3_RM	4_RM	2_RM	3_RM	4_RM	5_RM	6_RM	5_RM	6_RM	7_RM	8_RM	7_RM	8_RM
Max. stress [MPa]	4.85	4.33	4.39	5.74	4.95	4.19	5.25	5.43	5.13	6.41	5.75	5.18	6.30	6.16
(Av.)		(4.52)			(4.96)		(5.34)		(5.77)		(5.47)		(6.23)	
Max. axial strain [-]	0.37	0.39	0.38	0.55	0.56	0.82	0.0409	0.0403	0.0367	0.48	0.0502	0.0450	0.45	0.1111
(Av.)		(0.38)			(0.64)		(0.0406)		(0.0208)		(0.0476)		(0.0578)	
Ultimate stress [MPa]	4.02	3.44	3.51	-	-	-	-	-	-	-	-	-	-	-
(Av.)		(3.65)			-		-		-		-		-	
Ultimate axial strain [-]	4.59	4.13	3.53	-	-	-	-	-	-	-	-	-	-	-
(Av.)		(4.08)			-		-		-		-		-	
Max. hoop strain [-]	0.02	0.02	0.02	-	0.01	0.04	0.02	0.02	0.04	0.02	0.01	0.01	0.04	0.03
(Av.)		(0.02)			(0.03)		(0.02)		(0.03)		(0.01)		(0.04)	
First cracking stress [MPa]	2.69	2.79	1.58	1.43	2.10	2.50	3.74	3.80	4.53	5.36	3.40	4.46	5.13	4.11
(Av.)		(2.35)			(2.01)		(3.77)		(4.95)		(3.93)		(4.62)	
Elastic modulus [MPa]	1315	1894	2069	1370	1757	925	1210	1076	619	1102	993	1217	1485	492
(Av.)		(1759)			(1341)		(1143)		(860)		(1105)		(989)	
$\sigma_{Vmax,RM}/\sigma_{Vmax,URM}$	1.18	1.05	1.07	1.40	1.20	1.02	1.28	1.32	1.25	1.56	1.40	1.26	1.54	1.50

Unreinforced clay masonry

Fig. 17 shows the typical failure modes of unreinforced clay brick masonry columns tested by the four laboratories UniBo, UniCal, PoliMi, UniNa.

(a) (b)

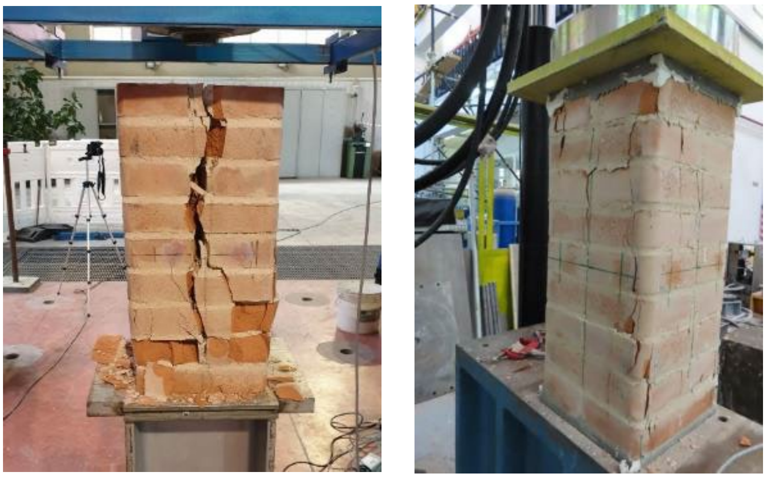

(c) (d)

Fig. 17. Unreinforced clay brick masonry specimens after testing: a) 1_URM PoliMi; b) 2_URM UniBo; c) 1_URM UniCal; d)1_URM UniNa .

All URM specimens showed similar failure modes, characterized by sub-vertical cracks developed along the longitudinal direction. Only the specimen tested by PoliMi (Fig. 17a) showed a slightly different failure mode. In particular, the crack appears to be more limited in a specific portion of masonry. This difference is probably due to lack of top and bottom capping layers. In fact, localized premature failures are enhanced without a regular top and bottom surface. Fig. 18 shows the axial stress as a function of the longitudinal and hoop strains experimentally obtained for the URM columns.

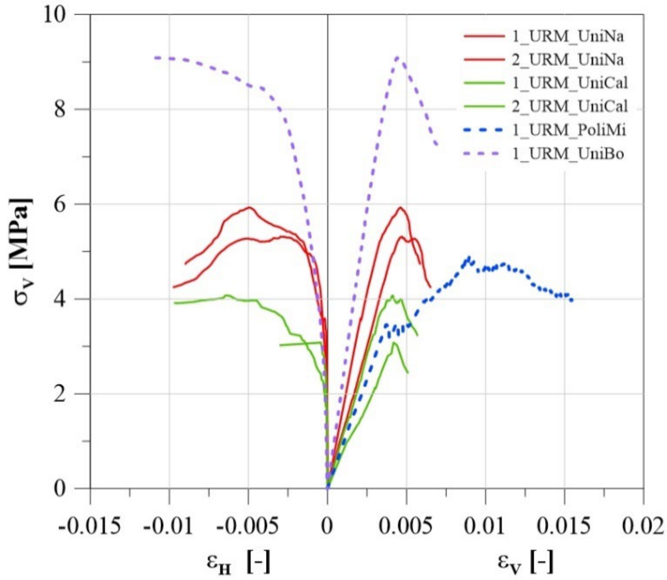

Fig. 18. Axial stress vs. axial and hoop strain for unreinforced clay brick masonry specimens.

Different repetitions of URM masonry columns have been considered for experimental tests by the four labs. One URM specimen was tested by PoliMi and UniBo (dotted curves of Fig. 18); while, two URM specimens were tested by UniNa and UniCal (solid curves of Fig. 18). The different behavior of the URM specimen tested by the PoliMi can be found also by observing the stress-strain law (Fig. 18). In particular, the specimen showed a conventional ultimate strain equal to 15.5‰ (dotted blue curve of Fig. 18), significantly higher than values achieved by the other URM columns (average value of 5.9‰). The load carrying capacities of URM specimens resulted compatible with the typical dispersion of masonry material. The columns manufactured at UniBo exhibited minimum and maximum axial stress values equal to 4.92 MPa and 9.09 MPa respectively. Conversely, for the specimens manufactured at UniSal the maximum axial stress ranges from 3.08 MPa to 5.93 MPa. The URM specimens tested by the UniCal lab have maximum axial stress about 35% lower than URM specimens tested by UniNa, but they did not test the specimens with the capping.

The URM specimens manufactured by UniBo (Fig. 18) show a variable initial stiffness, from 714 to 2391 MPa. Again, the minimum value was detected for the specimen tested by the PoliMi lab, for which no capping was realized, as already discussed (Fig. 17). For these specimens, the top and bottom surfaces were not regularized. In fact, the initial average stiffness is very close between the specimen tested by PoliMi and UniCal (blue curve of Fig. 18). Specimens tested by UniNa showed an average initial stiffness of about 1400 MPa. Full experimental results are reported in Table 9.

Table 9. Experimental results for unreinforced clay masonries.

Outputs	**UniNa**		**UniCal**		**PoliMi**	**UniBo**
	1_URM	**2_URM**	**1_URM**	**2_URM**	**1_URM**	**1_URM**
Maximum stress [MPa]	5.93	5.31	3.08	4.07	4.92	9.09
(Av.)	(4.60)				(7.01)	
Maximum axial strain [-]	0.46	0.47	0.42	0.41	0.80	0.44
(Av.)	(0.44)				(0.62)	
Ultimate stress [MPa]	4.74	4025	2.38	3.15	4.42	7.26
(Av.)	(3.63)				(5.84)	
Ultimate axial strain [-]	0.58	0.65	0.51	0.57	-	0.69
(Av.)	(0.58)				-	
Maximum hoop strain [-]	0.49	0.30	0.04	0.63	-	1.13
(Av.)	(0.37)				-	
First cracking stress [MPa]	3.55	2.69	2.05	1.47	3.48	-
(Av.)	(2.44)				(3.48)	
Elastic modulus [MPa]	1674	1173	714	1064	809	2391
(Av.)	(1156)				(16)	

Clay masonry confined by Glass Textile Reinforced Mortar (GFRCM)

The specimens wrapped by inorganic matrix-glass grid composites were manufactured by UniSal and later tested by UniNa and UniCal. The failure modes of the strengthened masonry columns are shown in Fig. 19. As seen for *Tuff* columns, the failure of the confined columns occurs when the tensile capacity of the fibres is reached, usually around the corner regions. In some cases the failure was also accompanied by buckling and debonding phenomena at mid height, along the vertical direction. This buckling phenomenon can be due to the shear stress developing at the ends of the specimen through the bond between the masonry and the external wrap.

Specimen tested by UniNa *Specimen tested by UniCal*

One layer GFRCM

Two layers GFRCM

Three layers GFRCM

Fig. 19. Failure mode of clay masonry specimens confined by GFRCM.

The increase of load carrying capacity, for all the considered cases, is reported in Fig. 20.

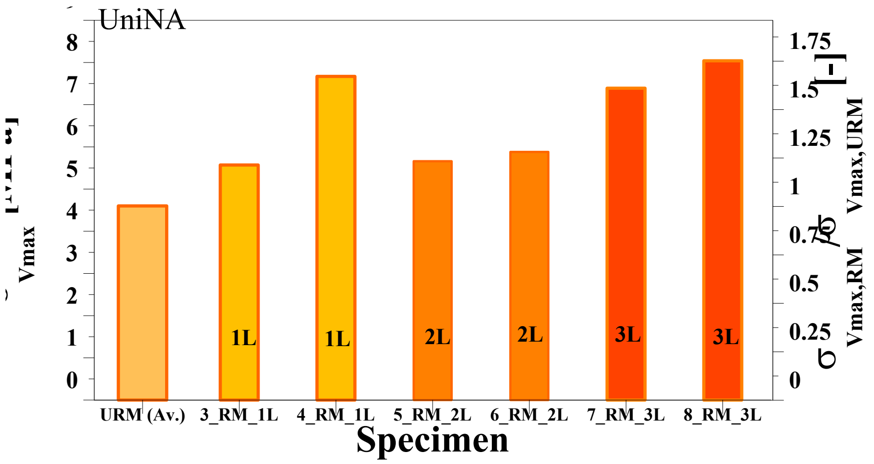

a)

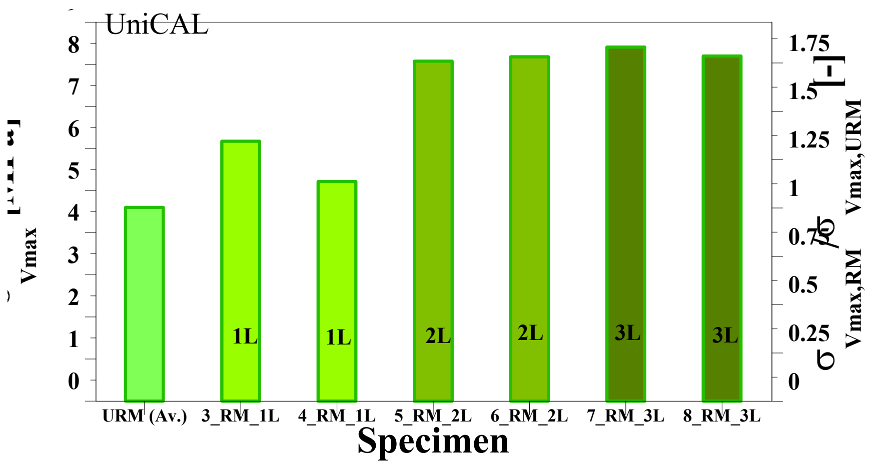

b)

Fig. 20. Maximum stress and dimensionless load carrying capacity of clay bricks masonry columns confined by GFRCM a) Specimens tested by UniNa; b) Specimens tested by UniCal.

Full experimental results are shown in Table 10.

Table 10. Experimental results for clay brick masonry columns strengthened by means of GFRCM systems.

Outputs	**Clay bricks**											
	1 layer				**2 layers**				**3 layers**			
	UniNa		**UniCal**		**UniNa**		**UniCal**		**UniNa**		**UniCal**	
	3_RM	4_RM	3_RM	4_RM	5_RM	6_RM	5_RM	6_RM	7_RM	8_RM	7_RM	8_RM
Max. stress [MPa]	5.57	7.67	6.17	5.22	5.66	5.88	8.07	8.18	7.39	8.04	8.41	8.20

(Av.)	(6.62)		(5.70)		(5.77)		(8.13)		(7.72)		(8.31)	
Max. axial strain [-]	0.41	0.66	0.66	0.51	0.55	0.53	0.72	0.67	0.77	0.79	0.59	0.59
(Av.)	(0.54)		(0.59)		(0.54)		(0.70)		(0.78)		(0.59)	
Ultimate stress [MPa]	4.45	6.13	4.78	4.21	4.53	4.70	6.28	6.67	5.91	6.43	6.44	5.62
(Av.)	(5.29)		(4.50)		(4.62)		(6.48)		(6.17)		(6.03)	
Ultimate axial strain [-]	0.70	0.82	0.86	0.61	0.69	0.62	0.80	0.80	0.0111	0.98	0.74	0.74
(Av.)	(0.76)		(0.73)		(0.65)		(0.80		(0.0104)		(0.74)	
Max. hoop strain [-]	0.58	0.0131	0.0248	0.0145	0.0152	0.95	0.0204	0.78	0.0126	0.0128	0.47	0.90
(Av.)	(0.95)		(0.0197)		(0.0124)		(0.0141)		(0.0127)		(0.69)	
First cracking stress [MPa]	3.072	3.28	2.07	2.04	3.30	4.19	2.58	3.01	5.04	5.63	3.01	3.06
(Av.)	(3.18)		(2.06)		(3.75)		(2.80)		(5.34)		(3.04)	
Elastic modulus [MPa]	2202	1858	1082	1398	2254	2755	1245	1340	2926	2669	1637	1925
(Av.)	(2030)		(1240)		(2505)		(1293)		(2798)		(1781)	
$\sigma_{Vmax,RM}/\sigma_{Vmax,URM}$	1.23	1.69	1.32	1.11	1.24	1.29	1.73	1.75	1.62	1.77	1.80	1.75

The behavior of confined specimens in terms of peak load is reported in Fig. 20. The effectiveness of wrapping reinforcement becomes more apparent for two- and three-layers cases for columns tested by UniCal, while for tests carried out by UniNa lower variation of the peak-load have been obtained varying the number of layers. However, the behavior of confined specimens (Fig. 20) is characterized by a strong dispersion in terms of load carrying capacity, which reduces as the amount of confining reinforcement increases. Fig. 21 shows experimental curves in terms of axial stress *vs* axial and transverse strains for all the tested specimens. After the peak stress, all the columns showed a brittle softening behavior.

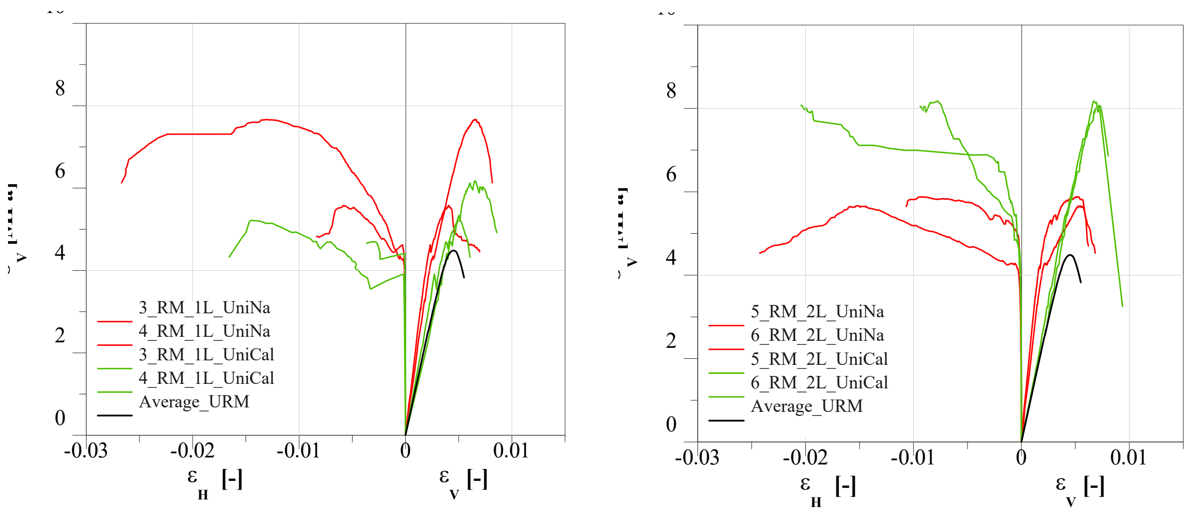

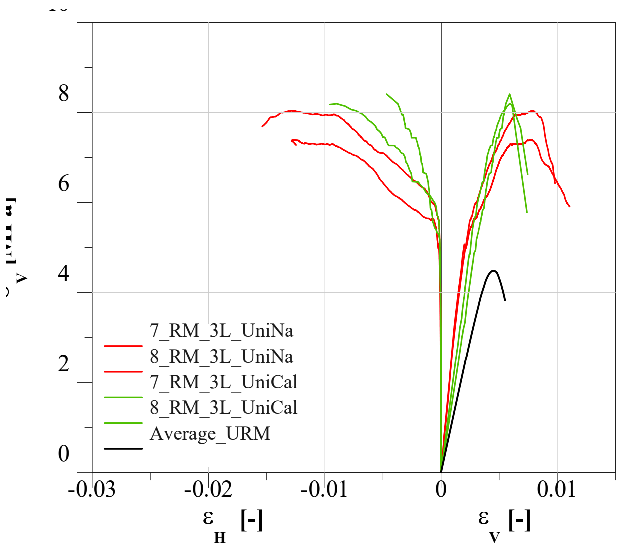

Fig. 21. Axial stress vs. axial and hoop strain for clay brick masonry specimens confined by GFRCM systems. a) Specimens confined with one layer; b) Specimens confined with two layers; c) Specimens confined with three layers.

The results obtained by UniNa (red curves of Fig. 21) showed significant issues related to the efficiency of the strengthening system. In particular, low number of layers could lead to poor confinement performance. It has been confirmed by the strong dispersion detected for columns confined by 1-layer of GFRCM. The maximum axial stress ranges from 5.57 MPa to 7.67 MPa (red curves Fig. 21a) where, the first value is very similar to the capacity of URM specimens, while the second is comparable with the specimen confined by 3-layers (red curves Fig. 21c). For specimens strengthened with 2-layers system, the load carrying capacity results weakly increased (5.66 and 5.88 MPa) (red curves of Fig. 21b) with respect to that of unconfined specimens. Conversely, the 3-layers systems showed a clear beneficial effect in terms of load carrying capacity (7.39 and 8.04 MPa).

The specimens tested by UniCal exhibited an almost constant load carrying capacity for specimens reinforced with 2 and 3 layers (green curves in Fig. 21b and c). The specimens confined with 1-layer system (orange curves in Fig. 21a) present a maximum axial stress ranging from 5.22 MPa to 6.17 MPa while, the average value of other strengthened columns (2 and 3-layers system) is 8.2 MPa.

As also observed for the strength values, the elastic modulus (Fig. 21) reduces its dispersion by increasing the reinforcement amount. The stiffness of specimens tested by UniCal (green curves of Fig. 21) appears always lower than that of specimens tested by UniNa (red curves of Fig. 21). Experimental results showed average values of 2030, 2505 and 2800 MPa for the specimens tested by UniNa with one-, two- and three-layers' system, respectively. Conversely, the specimens tested by UniCal are characterized by an average stiffness of 1240, 1293 and 1781 MPa. As expected, the elastic modulus progressively increases with the amount of reinforcement, due to the additional contribution of composite and the reduced capacity of lateral expansion.

The ultimate longitudinal axial strain of specimens tested by UniCal appears to be weakly influenced by the amount of reinforcement (approximately 7‰ – green curves of Fig. 21). However, this aspect is probably due to the smaller reliability of measurements of the axial displacement after the attainment of the peak stress. In fact, for the confined columns, the LVDT devices were placed on the wrapped surface; therefore, especially once the peak-state was exceeded, a probable slip between the internal masonry and composite may promote measurement errors. This effect is less marked for axial deformations at the peak stress

The ultimate deformations detected for the specimens tested by UniNa (Fig. 21) confirmed what was highlighted by the analysis of the peak loads. The two unreinforced specimens and one specimen strengthened with a one-layer system exhibited very similar behavior while the remaining specimen strengthened with one-layer system, showed properties very close to specimens reinforced with three-layers system. Very small increases in capacity were also detected for systems reinforced with two layers, with respect to the unreinforced specimens. The three-layer systems instead showed a clear beneficial effect in terms of load capacity.

The maximum hoop strains at the peak load reduce as the number of layers increases (Fig. 21).

Clay masonry confined by Steel Reinforced Grout (SRG)

Clay brick masonry columns strengthened by SRG reinforcement were tested by UniBo and PoliMi, while they were all manufactured by UniBo. Fig. 22 shows the failure modes observed for the confined columns. The failure modes resulted very similar for all the tested samples (Fig. 22). The damage started from the edges for all specimens. Once the peak stress was exceeded, the external layer of the strengthening system showed a debonding phenomenon from the substrate or from the inner layer. This mechanism was observed starting from mid height of the wrapped surfaces (along the longitudinal axis).

Specimen tested by PoliMi | *Specimen tested by UniBo*

One layer SRG

Two layers SRG

Three layers

SRG

Fig. 22. Failure mode of clay brick masonry specimens confined by SRG.

Fig. 23 shows the increase in peak-stress of the confined masonry columns. Effectiveness of the wrapping system increases with the number of layers. It is also clear that the dispersion of results decreases with the amount of reinforcement.

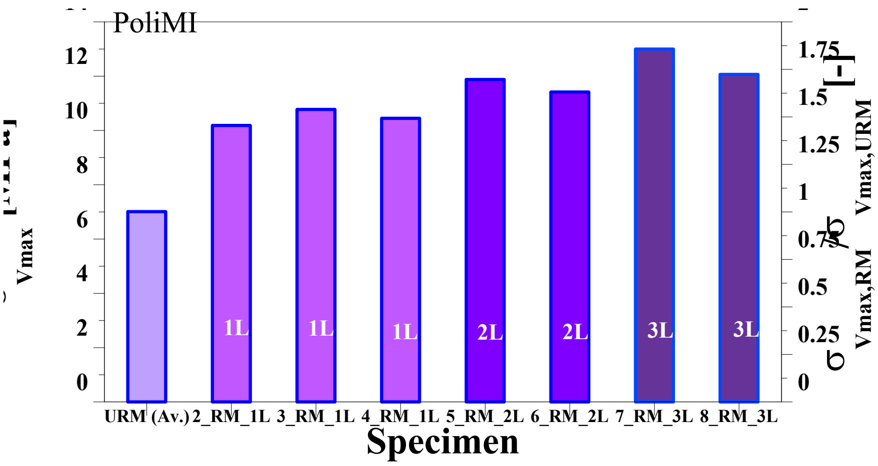

a)

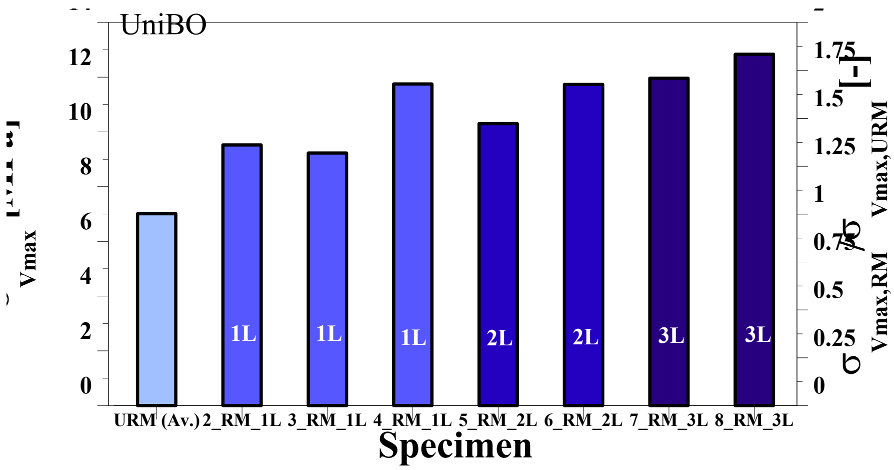

b)

Fig. 23. Maximum stress and dimensionless load carrying capacity of clay bricks masonry columns confined by SRG a) Specimens tested by PoliMi; b) Specimens tested by UniBo.

Furthermore, it is interesting to observe the complete axial stress-strain curve of each specimen and for the different number of layers (Fig. 24).

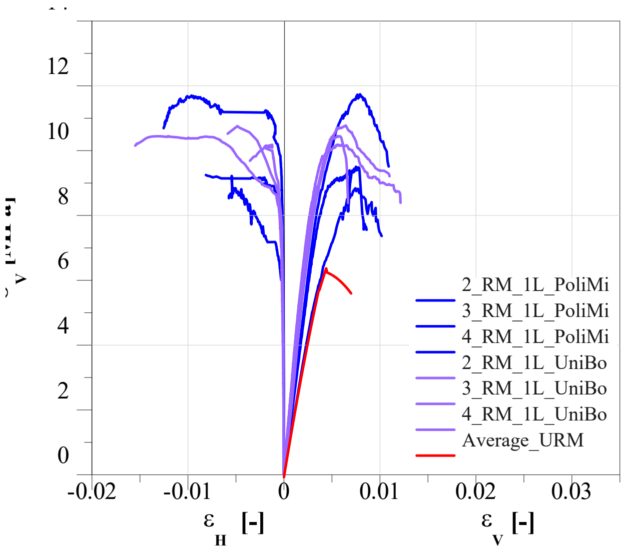

a)

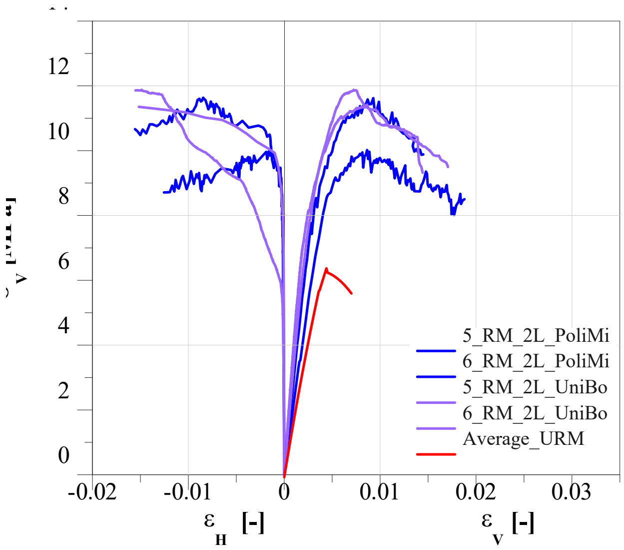

b)

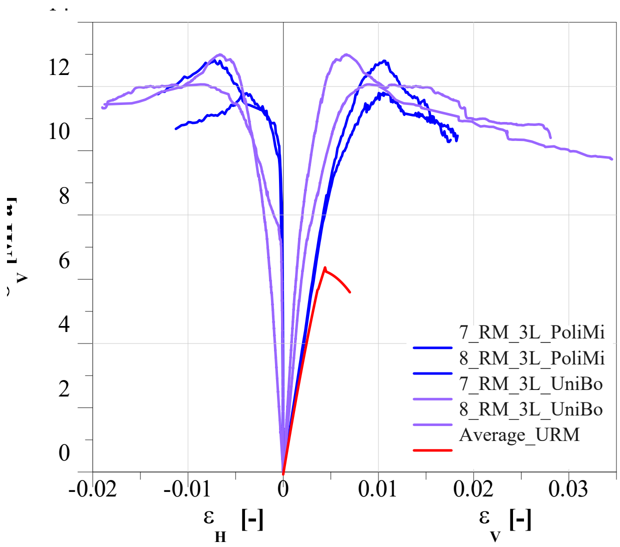

c)

Fig. 24. Axial stress vs. axial and hoop strain for clay masonry specimens confined by SRG. a) Specimens confined with one layer; b) Specimens confined with two layers; c) Specimens confined with three layers.

Curves become smoother by increasing the number of layers. In fact, the specimens wrapped by three-layers present a similar load carrying capacity and initial stiffness. For masonry columns wrapped by one-layer system the maximum axial stress ranges from 9.23 MPa (PoliMi) to 11.77 MPa (UniBo). Increasing the amount of fabric plies, the maximum axial stress ranges from 10.3 MPa (PoliMi) to 11.88 MPa (UniBo) and from 11.96 (PoliMi) to 13 MPa (UniBo) for two- and three-layer systems, respectively. The experimental tests carried out by UniBo (violet curves of Fig. 21) show a dispersion lower than the results by PoliMi. In fact, both the load carrying capacity and the ultimate strains values progressively increase with the number of layers. These results are affected by a small difference between one specimen and the other of the same type.

The initial stiffness values are more uniform if compared with those of the URM specimens. Experimental results showed average values of 2157, 2488 and 1901 MPa for the specimens tested by PoliMi with one-, two- and three-layers system, respectively. While the corresponding specimens tested by UniBo are characterized by an increasing average stiffness of 3365, 3702 and 3948 MPa. For these specimens, the equivalent elastic modulus seems to be weakly influenced by the strengthening system if compared with the specimens tested by PoliMi.

The specimens tested by UniBo, especially the 3-layer systems, have shown higher ultimate axial deformations with respect to those columns tested by PoliMi. The longitudinal strain, at the maximum axial stress, seems generally not influenced by the number of layers. On the other hand, the ultimate strain clearly increases with the amount of reinforcement ratio.

The axial stress-hoop strain curves (left part of graphs in Fig. 24) are probably affected by measurement issues due to the post-cracked state. However, the beneficial effect of confinement due to the composite is clear. The experimental results for clay masonry columns confined by means of SRG systems are shown in Table 11.

Table 11. Experimental results for clay brick masonry columns strengthened by means of SRG systems.

Outputs	**Clay bricks**													
	1 layer						**2 layers**				**3 layers**			
	PoliMi			**UniBo**			**PoliMi**		**UniBo**		**PoliMi**		**UniBo**	
	2_RM	3_RM	4_RM	2_RM	3_RM	4_RM	5_RM	6_RM	5_RM	6_RM	7_RM	8_RM	7_RM	8_RM
Max. stress [MPa]	9.52	9.23	11.75	10.18	10.77	10.45	10.30	11.73	11.88	11.42	11.96	12.84	13.	12.06
(Av.)		(10.17)			(10.47)		(11.02)		(11.65)		(12.40)		(12.53)	
Max. axial strain [-]	0.78	0.84	0.81	0.56	0.64	0.56	0.88	0.90	0.72	0.86	0.0101	0.0106	0.66	0.91
(Av.)		(0.81)			(0.59)		(0.89)		(0.79)		(0.0104)		(0.79)	
Ultimate stress [MPa]	7.56	7.32	9.34	8.32	9.25	8.38	8.16	9.34	9.38	9.06	10.42	10.33	10.36	9.46
(Av.)		(8.07)			(8.65)		(8.75)		(9.22)		(10.38)		(9.91)	
Ultimate axial strain [-]	0.87	0.0107	0.0116	0.121	0.0110	0.67	0.0188	0.0148	0.0170	0.0145	0.0184	0.0177	0.0280	0.0352
(Av.)		(0.0103)			(0.99)		(0.0168)		(0.0158)		(0.0180)		(0.0316)	
Max. hoop strain [-]	0.0118	0.54	0.85	0.12	0.49	0.0121	0.18	0.85	0.0149	0.0150	0.35	0.75	0.52	0.87
(Av.)		(0.86)			(0.61)		(0.52)		(0.0150)		(0.55)		(0.70)	
First cracking stress [MPa]	5.34	5.07	8.81	-	-	-	3.53	6.17	-	-	9.76	7.81	-	-
(Av.)		(6.41)			-		(4.85)		-		(8.79)		-	
Elastic modulus [MPa]	23	1731	2441	3983	2936	3177	2097	2879	3342	4061	1869	1933	4647	3248
(Av.)		(2157)			(3365)		(2488)		(3702)		(1901)		(3948)	
$\sigma_{Vmax,RM}/\sigma_{Vmax,URM}$	1.44	1.54	1.49	1.36	1.32	1.68	1.67	1.60	1.47	1.67	1.85	1.69	1.71	1.83

DESIGN CONSIDERATION

As evidenced by the above described experimental results, the axial response of a FRCM-confined masonry column is affected by cracks opening both into the core and within the jacket. For this reason, the analytical prediction of the axial strength cannot disregard the parameter related to the masonry, the fabric and the FRCM-matrix. All analytical models proposed so far to predict the axial strength of the FRCM confined masonry columns were developed according to this consideration; among those, the models by Krevaikas [47], Ramaglia et al. [54], Cascardi et al. [43], Italian CNR DT-215 [32] and ACI 549-R13 [15] guidelines. Even if derived from different approaches, the formulations proposed to predict the axial strength of confined masonry columns present a similar non-linear form. The main difference between the mentioned model predictions is related to the computation of the effective confinement pressure [55].

In the following, the Standards available to date, namely the Italian CNR DT 215 [32] and the American ACI549-R13 [15], are used for comparison with experimental results, in order to further check the effectiveness of the design relationship proposed for the confinement of masonry columns, mostly when the number of layers increases, considering that the already available experimental database on this aspect is very limited. The analytical formulations of the two models are summarized in Table 12.

Table 12. Comparison of the prediction models.

	ACI 549-R13 [15]	CNR DT 215 [32]
Compressive strength of the FRCM-confined column	$f_{mcd} = f_{md} + 3.1\, k_a f_l$	$f_{mcd} = f_{md}\left[1 + k'\left(\frac{k_H f_{l,eff}}{f_{md}}\right)^{\alpha_1}\right]$
k'	-	$k' = \alpha_2(\frac{g_m}{10})^{\alpha_3}$
Shape factor	$k_a = \frac{A_e}{A_c}\left(\frac{b}{h}\right)^2$ $\frac{A_e}{A_c} = 1 - \frac{\left[\left(\frac{b}{h}\right)(h-2r_c)^2 + \left(\frac{h}{b}\right)(h-2r_c)^2\right]}{3bh}$	-
α_1	-	0.5
α_2	-	1.0
α_3	-	1.0
Maximum confinement pressure	$f_l = \frac{2nA_f E_f \varepsilon_{fe}}{\sqrt{b^2+h^2}}$	
Effective confinement pressure	-	$f_{l,eff} = \frac{2nt_f E_f \varepsilon_{fe}}{\sqrt{b^2+h^2}}$
Horizontal geometrical efficiency coefficient	-	$k_H = 1 - \frac{(b-2r_c)^2 + (h-2r_c)^2}{3bh}$
Effective strain	$\varepsilon_{fe} = \varepsilon_{fd} \leq 0.012$	$\varepsilon_{fe} = \min\left(k_{mat}\eta_a \frac{\varepsilon_u}{\gamma_m}; 0.4\right)$
FRCM-matrix efficiency coefficient	-	$k_{mat} = 1.81\left(\rho_{mat}\frac{f_{c,mat}}{f_{md}}\right)^2$
Geometrical percentage of FRCM-matrix	-	$\rho_{mat} = \frac{4t_{mat}}{\sqrt{b^2+h^2}}$

For all tested specimens, the comparison between experimental results and predictions of the considered models in terms of maximum axial stress, $f_{c,m}$, are summarized in Tables 13-16 and Fig.s 25 and 26. Since the analytical relationships and predictions are used for comparison with experimental findings, the parameters introduced are the average values experimentally obtained and safety coefficients are not considered, thus the subscript "d" has been omitted for the utilized symbols.
Table 13 reports results obtained for the *Tuff* columns confined by GFRCM systems. The analysis of the results ensures that both models provide similar predictions for each confinement configuration, i.e. for each confinement ratio (A_f/A_c). For *Tuff* columns confined with one layer of GFRCM the predicted $f_{c,m}$ values are on average 12% and 16% higher than provide experimental ones, respectively for the CNR DT215 and ACI 549-R13 models. Referring to the specimens with three layers of GFRCM the experimental values are on average underestimated of about 20%. Generally, the two models provide accurate predictions in case of one- and two- layer systems, considering the scattering of the experimental results (CoV=16% and 12% for one- and two- layer systems, respectively), while they appear both conservative for the case of three- layers' configuration (CoV=8%).

Table 13. Tuff masonry columns strengthened by GFRCM systems: predicted/experimental comparison

Outputs	***Tuff***					
	1 layer		**2 layers**		**3 layers**	
	UniPa	**UniSal**	**UniPa**	**UniSal**	**UniPa**	**UniSal**
Experimental [MPa] *(Av.)*	2.59	2.48	3.14	3.74	4.33	4.68
Predicted CNR DT 215 [MPa]	2.82		3.14		3.30	
Pred./Exp. CNR DT215	1.09	1.14	1.	0.84	0.76	0.70
Predicted ACI 549-R13 [MPa]	2.86		3.28		3.71	
Pred./Exp. ACI 549-R13 [-]	1.12	1.19	1.05	0.88	0.86	0.79

The results of the comparison obtained for the *Tuff* columns confined by SRG systems are summarized in Table 14. For these columns the values of $f_{c,m}$ predicted by the ACI model are higher than those predicted by the DT 215 model. The difference between the predictions of the two models is increasing with the number of confining layers.

In particular, for *Tuff* columns confined by one layer of SRG the predicted $f_{c,m}$ values are on average 5% and 22% higher than experimental ones for the DT215 and ACI 549-R13 models, respectively. The ratio between the predicted values and experimental results increases with the number of confining layers; referring to DT 215 it results on average equal to 1.05 and 1.08 for columns confined by two- and three layers, respectively, while using the ACI model it is on average 1.33 and 1.54 for *Tuff* columns confined with 2 and 3 layers of SRG. As a consequence, predictions of the DT 215 model seem more accurate, considering that the CoV values of experimental results are 12%, 10% and 8% for one-, two- and three-layer systems, respectively.

Table 14. Tuff masonry columns strengthened by SRG systems: predicted/experimental comparison

Outputs	***Tuff***					
	1 layer		**2 layers**		**3 layers**	
	UniFi	**UniSa**	**UniFi**	**UniSa**	**UniFi**	**UniSa**
Experimental [MPa] *(Av.)*	4.52	4.96	5.34	5.77	5.47	6.23
Predicted CNR DT 215 [MPa]	4.97		5.89		6.29	
Pred./Exp. CNR DT215	1.10	1.	1.10	1.02	1.15	1.01
Predicted ACI 549-R13 [MPa]	5.73		7.35		8.96	
Pred./Exp. ACI 549-R13 [-]	1.27	1.17	1.37	1.30	1.64	1.44

The comparison between predictions and experimental results for all tested *Tuff* columns is also illustrated in Fig. 25, where the above considerations are clearly confirmed.

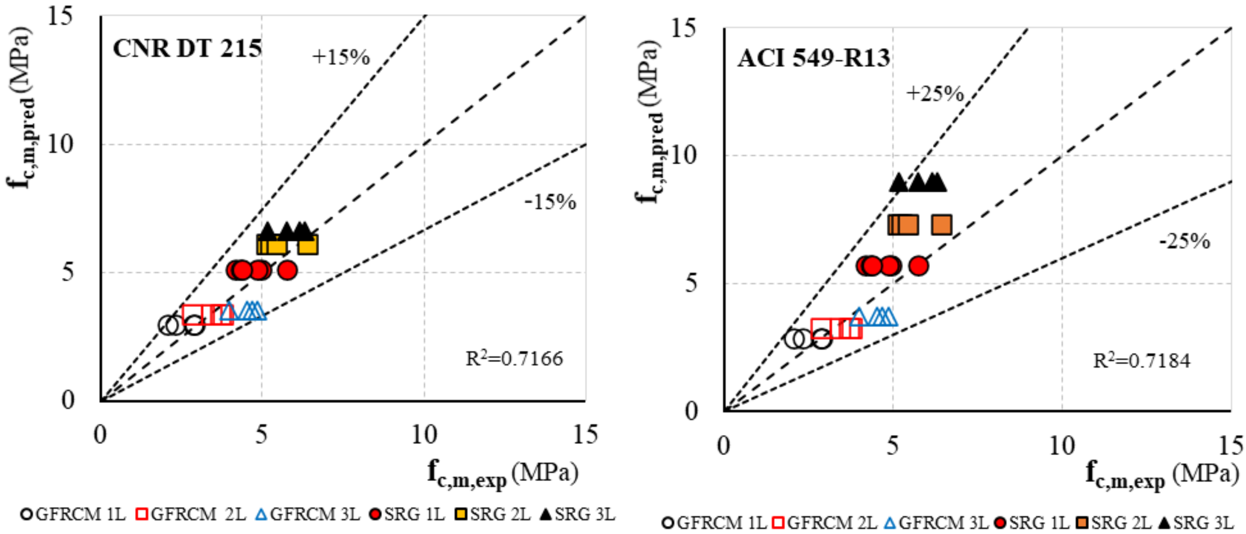

Fig. 25. Tuff masonry columns: predicted/experimental comparison

The comparison between model predictions and experimental results for the clay brick columns confined by GFRCM systems is summarized in Table 15. The obtained results show that the values of $f_{c,m}$ predicted by both considered models are similar and underestimate the experimental ones. However, considering the scatter of experimental results the two models appear highly conservative only for the three-layer configuration (COV= 18%, 20% and 5% for one-layer, two-layers and three-layers configuration, respectively).

Table 15. Clay brick masonry columns strengthened by means of GFRCM systems: predicted/experimental comparison

Outputs	Clay bricks					
	1 layer		2 layers		3 layers	
	UniNa	UniCal	UniNa	UniCal	UniNa	UniCal
Experimental [MPa] ***(Av.)***	6.62	5.70	5.77	8.13	7.72	8.31
Predicted CNR DT215 [MPa]	4.92		5.29		5.73	
Pred./Exp. CNR DT 215 [-]	0.76	0.83	0.91	0.65	0.74	0.69
Predicted ACI 549-R13 [MPa]	5.02		5.44		5.86	
Pred./Exp. ACI 549-R13 [-]	0.78	0.85	0.94	0.67	0.76	0.71

Table 16 summarizes the comparison between models' predictions and experimental results for clay brick columns confined by SRG systems. For these columns the average values of the ratio predicted/experimental results provided by the DT215 model is almost constant for each confinement ratio (0.75 for specimens confined with one, two and three layers of SRG). The predictions of the ACI model become more accurate with the number of confining layers; in fact, the ratio predicted/experimental results, is 0.83, 0.88 and 0.95 for specimens confined with one, two and three layers of SRG, respectively.

Table 16. Clay brick masonry columns strengthened by means of SRG systems: predicted/experimental comparison

Outputs	Clay bricks					
	1 layer		2 layers		3 layers	
	PoliMi	UniBo	PoliMi	UniBo	PoliMi	UniBo
Experimental [MPa] ***(Av.)***	10.17	10.47	11.02	11.65	12.40	12.53
Predicted CNR DT 215 [MPa]	7.67		8.42		9.32	
Pred./Exp. CNR DT 215 [-]	0.76	0.74	0.77	0.73	0.75	0.74
Predicted ACI 540-R13 [MPa]	8.62		10.24		11.86	

Pred./Exp ACI 549-R13 [-]	0.86	0.83	0.93	0.88	0.96	0.95

Fig. 26 reports the results of the comparison between predictions and experimental results for all tested clay brick columns. The analysis of the results confirms evidencing that the predictions of the two models are on average conservative, while the ACI formulation appears more accurate when referring to clay brick columns confined with SRG systems.

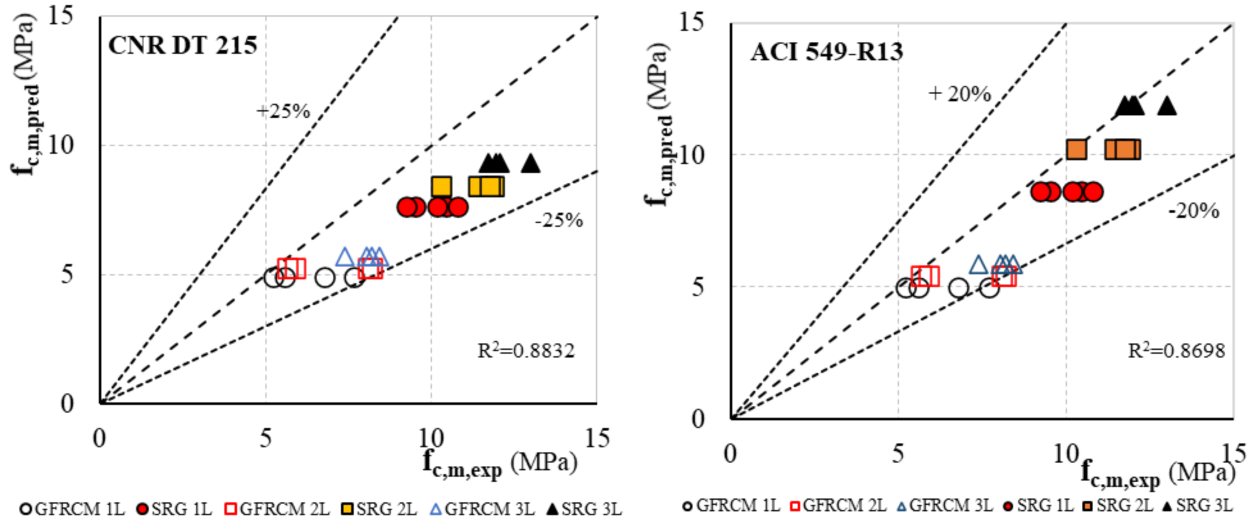

Fig. 26. Clay brick masonry columns: predicted/experimental comparison

Conclusions

In this paper, a Round Robin experimental activity on the mechanical behavior of masonry columns confined by using FRCM systems is reported and discussed. Eight Italian University laboratories were involved within the framework of the ReLUIS-DPC 2019–2021 project (WP 14) funded by the *Italian Department of Civil Protection*. Two reinforcing systems, namely GFRCM and SRG, were tested on two different kinds of masonry, *Tuff* stone and clay brick, considering three reinforcing configurations (one-layer, two-layers and three-layers of reinforcement). In total 64 specimens were tested. The obtained results were deeply analyzed and compared in order to gain new insight on the confinement, mainly referring to the effect of reinforcement configuration. The aim of this effort is valuable by considering that the available database is generally still limited when referring to the confinement of existing masonry columns by means of FRCMs and mostly when more than one layer is utilized for strengthening. The typical variability of masonry material, due to the influence of scatters characterizing both the constituent materials (mortar and stones), the variability of performances related to different manufacturing operators and the variability of utilized test setup from different laboratories, even if starting from the same agreed scheme, caused in some cases significant dispersion of experimental results. However, the carried out analysis can be considered very useful for the scientific community as well as for standards assessment and validation.

On the basis of obtained results the following considerations can be drawn:

- As regards the masonry specimens confined by GFRCM the failure mode was almost similar in all cases (*Tuff* stone and clay brick masonry), substantially characterized by the formation of one main critical crack in correspondence of the edge at one corner of the member, where as expected a stress concentration occurs, causing finally the mesh failure. SRG-confined *Tuff* masonry specimens showed a different failure, characterized by the formation of different cracks (horizontal and vertical direction), with final debonding of the reinforcement from the inner layer, mortar spalling or failure at the overlapping zones.
- The effectiveness of the confinement by using GFRCM increased with the numbers of layers for both kinds of tested masonry, even if following a different trend. In fact, in the case of *Tuff* masonry the one-layer configuration provided for a negligible improvement in terms of compressive strength, while the bearing capacity resulted almost 80% higher than that of reference specimens with three-layers of GFRCM, and the trend increase appears almost linear passing from one to two layers of reinforcement. As regards the clay-brick specimens an improvement of compressive strength was already registered

with one-layer reinforcement (34%) while increasing the number of composite layers the bearing capacity variation showed a reduced slope compared to the previous case, up to a bearing capacity increase of 74%, on average, for the case of three-layers configuration. This result remarks the influence of the mechanical properties of the composite in relation to those of the masonry; in fact, for a poor substrate the significant damage and, thus, the high expansion of the columns cannot be carried by the fibrous mesh of low density, typically used in FRCM systems. On the opposite, by increasing the reinforcement layers the confinement effectiveness increases as well attaining a relevant value. In the case of SRG systems confining clay bricks masonry the effectiveness of the confinement is higher than in the case of GFRM system even if similar values are attained, on average, for the two kinds of reinforcements in the case of three-layer configuration. On the other hand, when referring to *Tuff* masonry the greater benefit in case of SRG system is registered only with one-layer configuration. The increase in number of confining layers does not provide a proportional increase in effectiveness of confinement, probably due to the premature observed debonding phenomena. In addition, it can be observed that a higher deformability capacity is registered in all cases when the confinement is exerted by SRG systems, after the attainment of the maximum compressive stress. For all tested specimens the ultimate deformation registered on the composite is lower than that evaluated by tensile mechanical characterization; this result again confirms that in the case of FRCM/SRG systems a complex interaction between substrate, reinforcing textile and mortar matrix occurs; in particular, the mechanical properties of substrate/textile/mortar play a fundamental role, strongly affecting the proper activation of the passive confinement as well as the exploitation of its mechanical performances, the latter being influenced to a large extent also by the mortar properties.

- The obtained experimental results were used to understand the effectiveness of two available design-oriented formulas, reported in the Italian CNR (National Research Council) and ACI (American Concrete Institute) guidelines. Particular attention was devoted to check their effectiveness in case of multi-layers' reinforcement. The performed comparisons highlighted that the two design relationships provided for similar and accurate results when referring to the GFRCM system in one- and two- layer configurations, while the predictions appeared conservative when three- layers of GFRM are considered, irrespective of the type of masonry. Considering the SRG system, the results predicted by the two models are more scattered, mostly when the number of layers increases; in addition, the formulation proposed by CNR appears more accurate in case of *Tuff* masonry while the ACI predictions are closer to the experimental results in the case of clay brick masonry.

Further experimental programs are suggested in order to extend the available database to other kinds of reinforcement and masonry substrates, while considering a multi-ply configuration, in order to eventually address possible improvements of available design relationships.

Conflict of interest

The authors declare they to do not have any conflict of interest.

Acknowledgments

The authors sincerely thank the Italian Department of Civil Protection for funding the present research within the RELUIS program 2019-2021 (WP14- Contributions for Standards Assessment regarding the use of Innovative Materials for Strengthening Existing Structures). A special acknowledgment is also addressed to FibreNet s.p.a. and Kerakoll s.p.a. for providing their materials and technical support.

References

[1] International Federation for Structural Concrete (*fib*). Externally applied FRP reinforcement for concrete structures. fib Bulletin 90. International Federation for Structural Concrete (fib); 2019. https://doi.org/10.35789/fib.BULL.90.

[2] Micelli, F., & Cascardi, A. (2020). Structural assessment and seismic analysis of a 14th century masonry tower. Engineering Failure Analysis, 107, 104198.

[3] Wu, Z., Wang X., Zhao X., & Mohammad, N. (2014). State-of-the-art review of FRP composites for major construction with high performance and longevity Zhishen Int. J. Sustainable Materials and Structural Systems, 1(3), 201-231.

[4] Ascione, F., Lamberti, M., Napoli, A., Razaqpur, G., & Realfonzo, R. (2017). An experimental investigation on the bond behavior of steel reinforced polymers on concrete substrate. Composite Structures, 181, 58-72.

[5] Teng, J.G., Jiang, T., Lam, L., & Luo, Y.Z. (2009). Refinement of a design-oriented stress–strain model for FRP-confined concrete. Journal of Composites for Constructions; 13(4), 269–78.

[6] Ascione, F., Napoli, A., & Realfonzo, R. (2020). Interface bond between FRP systems and substrate: Analytical modeling. Composite Structures, Article number 112942 (in press).

[7] Babatunde, S.A. (2017). Review of strengthening techniques for masonry using fiber reinforced polymers. Composite Structures, 161, 246-255.

[8] Krevaikas, T.D., & Triantafillou, T.C. (2005). Masonry Confinement with Fiber-Reinforced Polymers. Journal of Composites for Construction, 9(2), 128–135.

[9] Faella, C., Martinelli, E., Camorani, G., Aiello, M.A., Micelli, F., & Nigro, E. (2011). Masonry columns confined by composite materials: Design formulae. Composites: Part B, 42, 705–716.

[10] Cascardi, A., Micelli, F., & Aiello, M. A. (2017). An Artificial Neural Networks model for the prediction of the compressive strength of FRP-confined concrete circular columns. Engineering Structures, 140, 199-208.

[11] Vaculik, J., Visintin, P., & Burton, N.G. (2018). Global database of FRP-to-masonry bond strength tests. Data in Brief, 20, 2065-2071.

[12] Cascardi, A., Leone, M., & Aiello, M. A. (2020). Transversal joining of multi-leaf masonry through different types of connector: Experimental and theoretical investigation. Construction and Building Materials, 265, 120733.

[13] Valluzzi, M. R. (2016). Challenges and perspectives for the protection of masonry structures in historic centers: the role of innovative materials and techniques. RILEM Technical Letters, 1, 45-49.

[14] ICOMOS/Iscarsah Committee. (25). Recommendations for the analysis, conservation and structural restoration of architectural heritage. See www.icomos.org

[15] ACI Committee 549. Guide to Design and construction of externally bonded fabric-reinforced cementitious matrix (FRCM) systems for repair and strengthening concrete and masonry structures; ACI 549.4R-13. ACI, Farmington Hill, US; 2013.

[16] Bencardino, F., Carloni, C., Condello, A., Focacci, F., Napoli, A., & Realfonzo, R. (2018). Flexural behaviour of RC members strengthened with FRCM: State-of-the-art and predictive formulas. Composites Part B: Engineering, 148, 132-148.

[17] Papanicolaou, C. G., Triantafillou, T. C., Papathanasiou, M., & Karlos, K. (28). Textile reinforced mortar (TRM) versus FRP as strengthening material of URM walls: out-of-plane cyclic loading. Materials and structures, 41(1), 143-157.

[18] Ascione, F., Lamberti, M., Napoli, A., & Realfonzo, R. (2020). Experimental bond behavior of Steel Reinforced Grout systems for strengthening concrete elements. Construction and Building Materials, 232.

[19] De Felice, G., De Santis, S., Realfonzo, R., Napoli, A., Ascione F., Stievanin, E., Cescatti, E., Valluzzi, M.R., Carloni, C., Santandrea, M., & Camata, G. (2018). State of the art of steel reinforced grout applications to strengthen masonry structures. American Concrete Institute, ACI Special Publication 2018, SP 326, 101.1-101.10.

[20] Campanini, D., Hadad, H. A., Carloni, C., Mazzotti, C., & Nanni, A. (2019). Mechanical Characterization of SRG Composites According to AC434. In Key Engineering Materials (Vol. 817, pp. 458-465). Trans Tech Publications Ltd.
[21] Cascardi, A., Micelli, F., & Aiello, M. A. (2016). Analytical model based on artificial neural network for masonry shear walls strengthened with FRM systems. Composites Part B: Engineering, 95, 252-263.
[22] D'Antino, T., Carozzi, F. G., Colombi, P., & Poggi, C. (2018). Out-of-plane maximum resisting bending moment of masonry walls strengthened with FRCM composites. Composite Structures, 202, 881-896.
[23] Alecci, V., Focacci, F., Rovero, L., Stipo, G., & De Stefano, M. (2017). Intrados strengthening of brick masonry arches with different FRCM composites: Experimental and analytical investigations. Composite Structures, 176, 898-909.
[24] Sneed, L. H., Baietti, G., Fraioli, G., & Carloni, C. (2019). Compressive Behavior of Brick Masonry Columns Confined with Steel-Reinforced Grout Jackets. Journal of Composites for Construction, 23(5), 04019037.
[25] Cascardi, A., Micelli, F., & Aiello, M. A. (2018). FRCM-confined masonry columns: experimental investigation on the effect of the inorganic matrix properties. Construction and Building Materials, 186, 811-825.
[26] Ombres, L., & Verre, S. (2018). Masonry columns strengthened with Steel Fabric Reinforced Cementitious Matrix (S-FRCM) jackets: Experimental and numerical analysis. Measurement, 127, 238-245.
[27] Di Ludovico, M., Cascardi, A., Balsamo, A., & Aiello, M. A. (2020). Uniaxial Experimental Tests on Full-Scale Limestone Masonry Columns Confined with Glass and Basalt FRCM Systems. Journal of Composites for Construction, 24(5), 040250.
[28] Ombres, L., & Verre, S. (2020). Analysis of the Behavior of FRCM Confined Clay Brick Masonry Columns. Fibers, 8(2), 11.
[29] Aiello, M.A.; Cascardi, A.; Ombres, L.; Verre, S. Confinement of Masonry Columns with the FRCM-System: Theoretical and Experimental Investigation. Infrastructures 2020, 5, 101.
[30] Micelli, F., Maddaloni, G., Longo, F., & Prota, A. Axial Stress–Strain Model for FRCM Confinement of Masonry Columns. Journal of Composites for Construction, 25(1), 040278.
[31] Cascardi, A., Dell'Anna, R., Micelli, F., Lionetto, F., Aiello, M. A., & Maffezzoli, A. (2019). Reversible techniques for FRP-confinement of masonry columns. Construction and Building Materials, 225, 415-428.
[32] National Research Council. Guide for the design and construction of externally bonded fibre reinforced inorganic matrix systems for strengthening existing structures. CNR-DT 215/2018. Rome, Italy, CNR, 2020.
[33] Carozzi, F. G., Bellini, A., D'Antino, T., de Felice, G., Focacci, F., Hojdys, Ł., ... & Poggi, C. (2017). Experimental investigation of tensile and bond properties of Carbon-FRCM composites for strengthening masonry elements. Composites Part B: Engineering, 128, 1-119.
[34] De Santis, S., Ceroni, F., de Felice, G., Fagone, M., Ghiassi, B., Kwiecień, A., ... & Viskovic, A. (2017). Round Robin Test on tensile and bond behaviour of Steel Reinforced Grout systems. Composites Part B: Engineering, 127, 1-120.
[35] Leone, M., Aiello, M. A., Balsamo, A., Carozzi, F. G., Ceroni, F., Corradi, M., ... & Mazzotti, C. (2017). Glass fabric reinforced cementitious matrix: Tensile properties and bond performance on masonry substrate. Composites Part B: Engineering, 127, 196-214.
[36] Lignola, G. P., Caggegi, C., Ceroni, F., De Santis, S., Krajewski, P., Lourenço, P. B., ... & Zuccarino, L. (2017). Performance assessment of basalt FRCM for retrofit applications on masonry. Composites Part B: Engineering, 128, 1-18.
[37] Caggegi, C., Carozzi, F. G., De Santis, S., Fabbrocino, F., Focacci, F., Hojdys, Ł., ... & Zuccarino, L. (2017). Experimental analysis on tensile and bond properties of PBO and aramid fabric reinforced cementitious matrix for strengthening masonry structures. Composites Part B: Engineering, 127, 175-195.

[38] Santandrea, M., Focacci, F., Mazzotti, C., Ubertini, F., Carloni, C. (2020). Determination of the interfacial cohesive material law for SRG composites bonded to a masonry substrate. Engineering Failure Analysis, 2020, 111, 104322.
[39] Carozzi, F. G., Bellini, A., D'Antino, T., de Felice, G., Focacci, F., Hojdys, Ł., ... & Poggi, C. (2017). Experimental investigation of tensile and bond properties of Carbon-FRCM composites for strengthening masonry elements. Composites Part B: Engineering, 128, 1-119.
[40] International Code Council Evaluation Service (ICC-ES). Acceptance criteria for masonry and concrete strengthening using fabric-reinforced cementitious matrix (FRCM) and steel reinforced grout (SRG) composite systems. AC434. Whittier, CA: 2018.
[41] Incerti, A., Vasiliu, A., Ferracuti, B., & Mazzotti, C. (2015, December). Uni-Axial compressive tests on masonry columns confined by FRP and FRCM. In Proc. of the 12th International Symposium on Fiber Reinforced Polymers for Reinforced Concrete Structures & The 5th Asia-Pacific Conference on Fiber Reinforced Polymers in Structures, Joint Conference, Nanjing, China, 14–16 December 2015.
[42] Cascardi, A., Aiello, M. A., & Triantafillou, T. (2017). Analysis-oriented model for concrete and masonry confined with fiber reinforced mortar. Materials and Structures, 50(4), 202.
[43] Cascardi, A., Longo, F., Micelli, F., & Aiello, M. A. (2017). Compressive strength of confined column with Fiber Reinforced Mortar (FRM): New design-oriented-models. Construction and Building Materials, 156, 387-401.
[44] Balsamo, A., Cascardi, A., Di Ludovico, M., Aiello, M. A., & Morandini, G. (2018). Analytical study on the effectiveness of the FRCM-confinement of masonry columns. In Construction Pathology, Rehabilitation. Technology and Heritage Management.
[45] Ombres L. Confinement effectiveness in eccentrically loaded masonry columns strengthened by fiber reinforced cementitious matrix (FRCM) jackets. In Vol. 624 of Key engineering materials, 551–558. Zurich, Switzerland: Trans Tech Publications.
[46] Murgo, F.S., Mazzotti, C. (2019). Masonry columns strengthened with FRCM system: Numerical and experimental evaluation. Construction and Building Materials, 2019, 202, pp. 208-222.
[47] Krevaikas, T. D. (2019). Experimental study on carbon fiber textile reinforced mortar system as a means for confinement of masonry columns. Construction and Building Materials, 208, 723-733.
[48] Fossetti, M., & Minafò, G. (2017). Comparative experimental analysis on the compressive behaviour of masonry columns strengthened by FRP, BFRCM or steel wires. Composites Part B: Engineering, 112, 112-124.
[49] EN 1015-11:27. Methods of test for mortar for masonry - Part 11: Determination of flexural and compressive strength of hardened mortar. CEN.
[50] EN 772-1:2011. Methods of test for masonry units - Part 1: Determination of compressive strength. CEN.
[51] UNI, Metodi di prova per pietre naturali–Determinazione della resistenza a compressione uniassiale, 27. [In Italian]
[52] EN ISO 13934_1:2013. Textiles — Tensile properties of fabrics — Part 1: Determination of maximum force and elongation at maximum force using the strip method.
[53] De Felice, G., Aiello, M. A., Caggegi, C., Ceroni, F., De Santis, S., Garbin, E., ... & Leone, M. (2018). Recommendation of RILEM Technical Committee 250-CSM: Test method for Textile Reinforced Mortar to substrate bond characterization. Materials and Structures, 51(4), 95.
[54] Ramaglia, G., Lignola, G. P., Fabbrocino, F., & Prota, A. (2019). Multi-parameters mechanical modeling to derive a confinement model for masonry columns. Construction and Building Materials, 214, 303-317.
[55] Lignola, G.P., Angiuli, R., Prota, A., Aiello, M.A. (2014). FRP confinement of masonry: analytical modeling. Materials and Structures, 47 (12), 2101-2115.